Title
Convergence Analysis of Triangular MAC Schemes for Two Dimensional Stokes Equations

Journal
Journal of Scientific Computing, 63(3)

ISSN
0885-7474

Authors
Chen, Long
Wang, Ming
Zhong, Lin

Publication Date
2015-06-01

DOI
10.1007/s10915-014-9916-z

Peer reviewed

HHS Public Access

Author manuscript

J Sci Comput. Author manuscript; available in PMC 2015 June 01.

Published in final edited form as:

J Sci Comput. 2015 June ; 63(3): 716–744. doi:10.1007/s10915-014-9916-z.

Convergence Analysis of Triangular MAC Schemes for Two Dimensional Stokes Equations

Long Chen,

Department of Mathematics, University of California at Irvine, Irvine, CA 92697, USA

Ming Wang, and

LMAM, School of Mathematical Sciences, Peking University, Beijing 100871, China

Lin Zhong

Department of Mathematics, University of California at Irvine, Irvine, CA 92697, USA

Long Chen: chenlong@math.uci.edu; Ming Wang: wangming.pku@gmail.com; Lin Zhong: lzhong1@uci.edu

Abstract

In this paper, we consider the use of $H(\mathrm{div})$ elements in the velocity–pressure formulation to discretize Stokes equations in two dimensions. We address the error estimate of the element pair RT_0–P_0, which is known to be suboptimal, and render the error estimate optimal by the symmetry of the grids and by the superconvergence result of Lagrange inter-polant. By enlarging RT_0 such that it becomes a modified BDM-type element, we develop a new discretization $\mathrm{BDM}_1^{\mathrm{b}} - \mathrm{P}_0$. We, therefore, generalize the classical MAC scheme on rectangular grids to triangular grids and retain all the desirable properties of the MAC scheme: exact divergence-free, solver-friendly, and local conservation of physical quantities. Further, we prove that the proposed discretization $\mathrm{BDM}_1^{\mathrm{b}} - \mathrm{P}_0$ achieves the optimal convergence rate for both velocity and pressure on general quasi-uniform grids, and one and half order convergence rate for the vorticity and a recovered pressure. We demonstrate the validity of theories developed here by numerical experiments.

Keywords

Stokes equations; $H(\mathrm{div})$ element; Exact divergence free

1 Introduction

We consider the steady-state Stokes equations

$$\begin{cases} -v\Delta \boldsymbol{u} + \operatorname{grad} p = \boldsymbol{f} & \text{in } \Omega, \\ -\operatorname{div} \boldsymbol{u} = 0 & \text{in } \Omega, \\ \boldsymbol{u} = \boldsymbol{g}_D & \text{on } \partial\Omega, \end{cases} \tag{1.1}$$

Correspondence to: Long Chen, chenlong@math.uci.edu.

where $\boldsymbol{u}$ is the velocity field, p the pressure, and $\boldsymbol{f}$ the external force field. In this paper, we will explore only the two-dimensional domain. For simplicity, we assume that Ω is simply connected and the Dirichlet boundary condition $\boldsymbol{g}_D = 0$.

The MAC scheme introduced by Harlow et al. [27] is a well known finite difference discretization of Stokes equations (1.1) on rectangular meshes. In particular, the MAC scheme is remarkable for its ability to enforce the incompressibility constraint of the velocity field point-wisely. It should also be noted that many efficient solvers, such as the distributive Gauss-Seidel (DGS) smoother based multigrid methods [6,41,47,48], have been devised for solving the corresponding saddle-point problem. Further, the MAC scheme has been shown to locally conserve the mass, momentum, kinetic energy, and circulation [42,43]. However, the standard MAC scheme is limited to rectangular meshes. To address this shortcoming, significant research effort has been dedicated to generalizing the MAC scheme to triangular meshes (TMAC).

Pioneering work on the TMAC discretization of Stokes equations dates back to Nédélec [35], who constructed a $H(\mathrm{div})$ element to approximate velocity. Since then, the TMAC scheme has been investigated using the finite volume methods approach [13,21,37], the finite element methods approach [18–20,23,24], and the discountinuous Galerkin (DG) approach [7,14,15,45,46]. The MAC scheme can be interpreted within these approaches when the underlying grids are rectangular [23,26,30,34,37].

Very recently, an error analysis of a vorticity–velocity–pressure formulation has been presented using the finite element exterior calculus framework. The study [2] demonstrates that a loss of exactness of the underlying differential complex causes a decrease in the order of convergence for the pressure and the vorticity. In particular, for the lowest-order approximation, the pressure has only half order convergence on general unstructured grids. In practice, however, first-order convergence is observed for meshes with good mesh quality and second-order for uniform grids [18–20]. In [12], we obtain a second-order convergence of the MAC scheme on uniform rectangular grids. In the present paper, we will investigate the convergence of TMAC schemes on general unstructured grids and mildly structured grids.

Although the vorticity–velocity–pressure formulation [18–20] seems a natural formulation when using $H(\mathrm{div})$ elements, we are interested in the more popular and traditional velocity–pressure formulation. In the velocity–pressure formulation, the vorticity will be eliminated in the discretization. In this way, we are able to reduce the size of the resulting linear algebraic equation, and thereby construct efficient multigrid solvers [47]. To eliminate vorticity, the inverse of the mass matrix for the vorticity element, which is in general a dense matrix, should be computed. Mass lumping will be applied to obtain a diagonal mass matrix so that the inverse is practical.

The main contributions of this paper are as follows:

1. We prove that the symmetry of the grids will improve the rate of convergence for the RT_0–P_0 element. The error analysis is closely related to the superconvergence results of the Lagrange interpolation of the linear element developed in [4]. More

precisely, suppose that the irregularity of the mesh is $\mathcal{O}(h^{2\sigma})$ (see Sect. 4 for a detailed definition).

We prove that

$$\|\omega-\omega_h\|+\|\boldsymbol{u}_{\mathrm{I}}-\boldsymbol{u}_h\|_{A_h}+\nu^{-1}\|p_{\mathrm{I}}-p_h\| \lesssim h^{\min(1,\sigma)}|\log h|^{1/2}(\|\boldsymbol{u}\|_{2,\infty}+\|\omega\|_2),$$

where $\boldsymbol{u}_{\mathrm{I}}$ is the canonical interpolation of $\boldsymbol{u}$ on to the space RT_0, p_I is the L^2 projection to P_0, $\boldsymbol{u}_h$ and p_h are the RT_0–P_0 approximation, ω is the vorticity and ω_h is the numerical approximation of ω based on $\boldsymbol{u}_h$, and $\|\cdot\|_{A_h}$ is a discrete version of the H^1-norm.

2. We propose a new velocity-pressure discretization $\mathrm{BDM}_1^{\mathrm{b}}-\mathrm{P}_0$. The velocity space is enriched to BDM_1 plus a cubic bubble function. This scheme maintains all the desirable properties of TMAC schemes; i.e., both schemes are divergence-free and solver-friendly, and can achieve local conservation. More importantly, it is both robust and more accurate than the RT_0–P_0 element and the error estimate can be improved to

$$\|\omega-\omega_h\|+\|\boldsymbol{u}_{\mathrm{I}}-\boldsymbol{u}_h\|_{A_h}+\nu^{-1}\|p_I-p_h\| \lesssim h^{1+\min(1/2,\sigma)}(\|\boldsymbol{u}\|_3+\|\boldsymbol{u}\|_{2,\infty}+\|\omega\|_3).$$

For general quasi-uniform but unstructured grids, the $\mathrm{BDM}_1^{\mathrm{b}}-\mathrm{P}_0$ scheme will produce an optimal first-order approximation for $\boldsymbol{u}$ and p and a one and half order approximation for vorticity. Further, we can recover a linear pressure approximation that has one and half order convergence.

3. Since point-wise divergence free elements are used to approximate the velocity, the right-hand side of our error estimates is independent of the pressure and the viscosity. For weakly divergence free elements, e.g., the popular Taylor-Hood elements [44], the term $\nu^{-1}\|p-p_I\|$ will appear in the right-hand side, which might be large when the pressure gradient is large or ν is small (i.e. the Reynolds number is large).

4. We present a new proof of the stability of the mixed finite element discretization of the vector Laplacian by establishing a discrete Poincaré inequality.

The paper is organized as follows. In Sect. 2, we introduce the TMAC discretization of the Stokes equations. In Sect. 3, we prove the stability of the TMAC scheme. In Sect. 4, we perform an error analysis of the TMAC scheme with an irregularity assumption on the meshes. We present numerical experiments in the last section.

We use $a \lesssim b$ to denote existence of a positive constant C independent of the mesh size h, such that $a \le Cb$, and we use $a \eqsim b$ to denote $a \lesssim b \lesssim a$. Bold face is used to denote vectors.

2 Discretization of Stokes Equations in the H(div) Space

Let us recall the following Sobolev spaces on a two-dimensional domain Ω. In order to distinguish between the curl operator acting on the scalar function from that acting on the vector function, we denote, for scalar ω and vector $\boldsymbol{u} = [u, v]^t$, respectively, as follows

$$\operatorname{curl}\omega=(\partial_y\omega,-\partial_x\omega),\operatorname{rot}\boldsymbol{u}=\partial_x v-\partial_y u.$$

Note that curl = grad$^{\perp}$ and that rot $\boldsymbol{u}$ = div $\boldsymbol{u}^{\perp}$. Here $\perp$ refers to a 90° degree clockwise rotation. We then introduce the following spaces on Ω:

$$H(\operatorname{curl})=\{u\in L^2(\Omega):\operatorname{curl}u\in\boldsymbol{L}^2(\Omega)\},H_0(\operatorname{curl})=\{u\in H(\operatorname{curl}):u=0\text{ on }\partial\Omega\},$$
$$\boldsymbol{H}(\operatorname{div})=\{\boldsymbol{u}\in\boldsymbol{L}^2(\Omega):\operatorname{div}\boldsymbol{u}\in L^2(\Omega)\},\boldsymbol{H}_0(\operatorname{div})=\{\boldsymbol{u}\in\boldsymbol{H}(\operatorname{div}):\boldsymbol{u}\cdot\boldsymbol{n}=0\text{ on }\partial\Omega\},$$
$$\boldsymbol{H}_0^1=\{\boldsymbol{u}\in\boldsymbol{H}^1(\Omega):\boldsymbol{u}=0\text{ on }\partial\Omega\},L_0^2=\{u\in L^2(\Omega):\textstyle\int_\Omega u dx=0\}.$$

As curl is a rotation of grad, $H(\operatorname{curl})\approxeq H^1$ and $H_0(\operatorname{curl})\cong H_0^1$. The inner product for L^2 or $\boldsymbol{L}^2$ is denoted by $(\cdot,\cdot)$.

2.1 The Velocity–Pressure Formulation of Stokes Equations using *H*(div) Elements

The velocity–pressure formulation of Stokes equations (1.1) considered here is based on this observation: for $\boldsymbol{u}\in\boldsymbol{H}_0^1$, the following identity holds in H^{-1} topology:

$$-\Delta\boldsymbol{u}=\operatorname{curl}\ \operatorname{rot}\boldsymbol{u}-\operatorname{grad}\ \operatorname{div}\boldsymbol{u}.$$

Then a weak formulation of the Stokes equations (1.1) seeks $(\boldsymbol{u},p)\in\boldsymbol{H}_0^1\times L_0^2$ satisfying

$$\begin{cases}\nu a(\boldsymbol{u},\boldsymbol{v})+b(\boldsymbol{v},p)=(\boldsymbol{f},\boldsymbol{v}) & \text{for all }\boldsymbol{v}\in\boldsymbol{H}_0^1,\\ b(\boldsymbol{u},q)=0 & \text{for all }q\in L_0^2,\end{cases}\quad(2.1)$$

where the bilinear forms $a(\cdot,\cdot)$ and $b(\cdot,\cdot)$ are defined as

$$a(\boldsymbol{u},\boldsymbol{v}):=(\operatorname{rot}\boldsymbol{u},\operatorname{rot}\boldsymbol{v})+(\operatorname{div}\boldsymbol{u},\operatorname{div}\boldsymbol{v})\text{ for all }\boldsymbol{u},\boldsymbol{v}\in\boldsymbol{H}_0^1,\quad(2.2)$$

$$b(\boldsymbol{v},q):=-(\operatorname{div}\boldsymbol{v},q)\text{ for all }\boldsymbol{v}\in\boldsymbol{H}_0^1,q\in L_0^2.\quad(2.3)$$

In order to obtain a discretization of the weak formulation (2.1), it is necessary to choose appropriate discrete spaces to approximate spaces $\boldsymbol{H}_0^1$ and L_0^2. Let $\mathcal{T}_h$ be a shape regular mesh of the domain Ω. Suppose that $\Sigma^h\subset H(\operatorname{curl})$, $\sum_0^h\subset H_0(\operatorname{curl})$, $\boldsymbol{V}_0^h\subset\boldsymbol{H}_0(\operatorname{div})$ and $S_0^h\subset L_0^2$ are appropriate discrete subspaces based on $\mathcal{T}_h$.

Definition 1 The linear operator $\mathrm{rot}_{0,h}: \boldsymbol{V}_0^h \to \sum_0^h$ is defined as follows: for a given $\boldsymbol{u} \in \boldsymbol{V}_0^h$, $\mathrm{rot}_{0,h}\boldsymbol{u} \in \sum_0^h$ such that

$$(\mathrm{rot}_{0,h}\boldsymbol{u}, \tau) = (\boldsymbol{u}, \mathrm{curl}\,\tau) \text{ for all } \tau \in \sum_0^h. \quad (2.4)$$

The linear operator $\mathrm{rot}_h : \boldsymbol{V}^h \to \sum^h$ is defined as follows: for a given $\boldsymbol{u} \in \boldsymbol{V}^h$, $\mathrm{rot}_h\boldsymbol{u} \in \sum^h$ such that

$$(\mathrm{rot}_h\boldsymbol{u}, \tau) = (\boldsymbol{u}, \mathrm{curl}\,\tau) \text{ for all } \tau \in \sum^h. \quad (2.5)$$

The linear operator $\mathrm{grad}_h: S_0^h \to \boldsymbol{V}_0^h$ is defined as: for a given $p \in S_0^h$, $\mathrm{grad}_h p \in \boldsymbol{V}_0^h$ such that

$$(\mathrm{grad}_h p, \boldsymbol{v}) = -(p, \mathrm{div}\,\boldsymbol{v}) \text{ for all } \boldsymbol{v} \in \boldsymbol{V}_0^h. \quad (2.6)$$

The operators $\mathrm{rot}_{0,h}$, rot_h and grad_h are well defined, since all these three systems are non-singular finite dimensional square systems.

The normal boundary condition $\boldsymbol{u} \cdot \boldsymbol{n} = 0$ is build into the space, whereas the tangential boundary condition $\boldsymbol{u} \cdot \boldsymbol{t} = 0$ is imposed weakly by the definition of weak rot operator rot_h; see (2.5). We will mainly apply rot_h to $\boldsymbol{V}_0^h \subset \boldsymbol{V}^h$. Note that $\mathrm{rot}_h|_{\boldsymbol{V}_0^h} \neq \mathrm{rot}_{0,h}$. Applying $\mathrm{rot}_{0,h}$ to $\boldsymbol{V}_0^h$ will enforce a boundary condition to the vorticity, which conflicts with the setting of the Stokes equations, i.e., no boundary condition of the vorticity is given.

With the help of operator rot_h, we define the discrete bilinear form $a_h(\cdot, \cdot)$ on the discrete space $\boldsymbol{V}_0^h$ as

$$a_h(\boldsymbol{u}, \boldsymbol{v}) := (\mathrm{rot}_h\boldsymbol{u}, \mathrm{rot}_h\boldsymbol{v}) + (\mathrm{div}\,\boldsymbol{u}, \mathrm{div}\,\boldsymbol{v}) \text{ for } \boldsymbol{u}, \boldsymbol{v} \in \boldsymbol{V}_0^h \quad (2.7)$$

Hence, a discrete formulation of (2.1) seeks $(\boldsymbol{u}_h, p_h) \in \boldsymbol{V}_0^h \times S_0^h$ such that:

$$\begin{cases} \boldsymbol{v}a_h(\boldsymbol{u}_h, \boldsymbol{v}_h) + b(\boldsymbol{v}_h, p_h) = (\boldsymbol{f}, \boldsymbol{v}_h) & \text{for all } \boldsymbol{v}_h \in \boldsymbol{V}_0^h, \\ b(\boldsymbol{u}_h, q_h) = 0 & \text{for all } q_h \in S_0^h. \end{cases} \quad (2.8)$$

Here $a_h(\cdot, \cdot)$ indicates that (2.8) is a nonconforming discretization of $a(\cdot, \cdot)$. However, the divergence-free constraint is imposed point-wisely. The traditional finite element method uses a conforming discretization of $a(\cdot, \cdot)$, but with this method it is not easy to impose the exact divergence-free constraint. A recent attempt to construct conforming and point-wise divergence-free finite elements on general triangular grids can be found in [22,25].

To compute rot_h, the mass matrix of space Σ^h should be inverted. This is not practical since the inverse of the mass matrix is dense. Therefore we will use mass lumping to approximate rot_h on the discrete space Σ^h. Equivalently, the L^2 inner product will be changed to a discrete one. More precisely, for $\rho,\ \tau \in \Sigma^h$,

$$\langle \rho, \tau \rangle = \sum_{i=1}^{n} \omega_i \rho(x_i)\tau(x_i), \quad (2.9)$$

where $\{x_i, i = 1, \cdots, n\}$ denote the quadrature points, n denotes the number of quadrature points of the triangulation, and $\{w_i, i = 1, \cdots, n\}$ are the corresponding integration weights. The quadrature should be chosen such that the mass matrix is diagonal for some bases, and $\langle \cdot, \cdot \rangle$ is an accurate enough approximation of $(\cdot, \cdot)$.

Definition 2 The linear operator $\widetilde{\mathrm{rot}}_h : \boldsymbol{V}^h \to \sum^h$ is defined as follows: for a given $\boldsymbol{u} \in \boldsymbol{V}^h$, $\widetilde{\mathrm{rot}}_h \boldsymbol{u} \in \sum^h$ such that

$$\langle \widetilde{\mathrm{rot}}_h \boldsymbol{u} : \tau \rangle = (\boldsymbol{u}, \mathrm{curl}\, \tau) \text{ for all } \tau \in \sum^h, \quad (2.10)$$

where $\langle \cdot, \cdot \rangle$ is the discrete L^2 inner product (2.9).

With the help of operator $\widetilde{\mathrm{rot}}_h$, we define the bilinear form $\tilde{a}_h(\cdot, \cdot)$ on the discrete space $\boldsymbol{V}_0^h$ as

$$\tilde{a}_h(\boldsymbol{u}, \boldsymbol{v}) := (\widetilde{\mathrm{rot}}_h \boldsymbol{u}, \widetilde{\mathrm{rot}}_h \boldsymbol{v}) + (\mathrm{div}\, \boldsymbol{u}, \mathrm{div}\, \boldsymbol{v}), \text{ for } \boldsymbol{u}, \boldsymbol{v} \in \boldsymbol{V}_0^h.$$

Remark 1 We can also define the bilinear form as

$$\tilde{a}_h(\boldsymbol{u}, \boldsymbol{v}) := \langle \widetilde{\mathrm{rot}}_h \boldsymbol{u}, \widetilde{\mathrm{rot}}_h \boldsymbol{v} \rangle + (\mathrm{div}\, \boldsymbol{u}, \mathrm{div}\, \boldsymbol{v}),$$

which is easier to implement. The stability and error estimates can be proved similarly.

Then a discrete formulation of (2.1) seeks $(\boldsymbol{u}_h, p_h) \in \boldsymbol{V}_0^h \times S_0^h$ such that

$$\begin{cases} \nu \tilde{a}_h(\boldsymbol{u}_h, \boldsymbol{v}_h) + b(\boldsymbol{v}_h, p_h) = (\boldsymbol{f}, \boldsymbol{v}_h) & \text{for all } \boldsymbol{v}_h \in \boldsymbol{V}_0^h, \\ b(\boldsymbol{u}_h, q_h) = 0 & \text{for all } q_h \in S_0^h. \end{cases} \quad (2.11)$$

2.2 Two Specific Discretizations of Stokes Equations

We now discuss appropriate discrete subspaces $\Sigma^h \subset H(\mathrm{curl})$, $\boldsymbol{V}_0^h \subset \boldsymbol{H}_0(\mathrm{div})$, and $S_0^h \subset L_0^2$, which are critical for the stability of the discretization. Given an integer $r \geq 1$, a stable

method is achieved by choosing Σ^h as the Lagrange element of degree r, $\boldsymbol{V}_0^h$ as the Raviart-Thomas element RT_{r-1}, and S_0^h as the discontinuous piecewise polynomial function space of degree $r - 1$. The case $r = 1$ corresponds to the lowest-order elements discretization, i.e., P_1–RT_0–P_0.

Another method relies on choosing Σ^h as the Lagrange element of degree $r + 1$, $\boldsymbol{V}_0^h$ as the Brezzi–Douglas–Marini element BDM_r, and S_0^h as the discontinuous piecewise polynomial function space of degree $r - 1$. The case $r = 1$ corresponds to the lowest-order element in this sequence, i.e., P_2–BDM_1–P_0.

In this paper, we will consider the simplest elements in each sequence, i.e., P_1–RT_0–P_0 and P_2–BDM_1–P_0, for which mass lumping is relatively easy.

2.2.1 RT_0–P_0 Element Discretization—First, we consider the pair P_1–RT_0–P_0. The bases of P_1 are the lowest-order continuous Lagrange element associated with each vertex. For a triangle τ, denote V_i ($i = 1, 2, 3$) as its three vertices. With the trapezoidal quadrature rule

$$\int_\tau f\,dx \approx \frac{|\tau|}{3}\sum_{i=1}^{3} f(V_i),$$

the lumped local mass matrix of P_1 element is diagonal:

$$M_\tau = |\tau|\,\mathrm{diag}\left(\frac{1}{3}, \frac{1}{3}, \frac{1}{3}\right).$$

Consequently the global mass matrix is also diagonal.

Let $\{\lambda_i, i = 1, 2, \cdots, N\}$ denote the linear nodal bases functions, where N is the number of vertices. The basis of RT_0, φ_k on edge e_{ij}, is given by

$$\phi_k = \lambda_i \mathrm{curl}\,\lambda_j - \lambda_j \mathrm{curl}\,\lambda_i.$$

The basis of P_0 is chosen as the characteristic function of each element τ. Given these bases, the matrix representation of the curl operator from P_1 to RT_0 is the incidences matrix between the edges and vertices, and the div matrix from RT_0 to P_0 is the incidences matrix between the triangles and edges.

Remark 2 When the triangulation is Delaunay, the mass matrix of RT_0 can be lumped with the help of circumcenters of triangles [5]. In this case, the discretization is identical to the co-volume method developed by Nicolaides [36,37], which in the rectangular case is

precisely the MAC scheme. The current finite element formulation, however, does not require the mesh to be Delaunay.

2.2.2 $\mathrm{BDM}_1^{\mathrm{b}} - \mathrm{P}_0$ **Element Discretization—**We consider the pair P_2–BDM_1–P_0. On each element τ, we have six nodal bases for P_2:

$$\theta_1=\lambda_1(2\lambda_1-1), \theta_2=\lambda_2(2\lambda_2-1), \theta_3=\lambda_3(2\lambda_3-1), \eta_1=4\lambda_2\lambda_3, \eta_2=4\lambda_3\lambda_1, \eta_3=4\lambda_1\lambda_2.$$

To maintain accuracy, the quadrature formula must be exact for quadratic functions. This can be achieved by using quadrature at the middle point of each edge. However, this quadrature yields a singular diagonal matrix, i.e., the rows corresponding to the unknowns at vertices are zero, as θ_i vanishes at these points. One way to resolve this is to add the bubble function $\omega_b = 27\lambda_1\lambda_2\lambda_3$ to P_2 element [16]. We construct $\hat{\theta_i}$ associated with vertices V_i and $\hat{\eta_i}$ associated with edges E_i vanishing at the barycenter C_τ of the triangle by

$$\hat{\theta}_i=\theta_i+\frac{1}{9}\omega_b, \hat{\eta}_i=\eta_i-\frac{4}{9}\omega_b, i=1,2,3.$$

Then a quadrature is obtained by expanding a quadratic function in the bases $(\hat{\theta_i}, \hat{\eta_i}, \hat{\omega_b})$, i.e., $f \approx \sum_{i=1}^{3} f(V_i)\hat{\theta}_i+\sum_{i=1}^{3} f(E_i)\hat{\eta}_i+f(C_\tau)\omega_b$ and applying the integral formula of each basis to get

$$\int_\tau f\,dx \approx |\tau|\left[\frac{1}{20}\sum_{i=1}^{3} f(V_i)+\frac{2}{15}\sum_{i=1}^{3} f(E_i)+\frac{9}{20}f(C_\tau)\right].$$

This quadrature is exact for $f \in P_2$ since $\mathrm{P}_2 \subset \mathrm{P}_2^{\mathrm{b}} := \mathrm{span}\{\hat{\theta}_i, \hat{\eta}_i, \omega_b, i=1,2,3\}$.

The element-wise mass matrix for $\mathrm{P}_2^{\mathrm{b}}$ is thus given by

$$M_\tau=|\tau|\mathrm{diag}\left(\frac{1}{20}, \frac{1}{20}, \frac{1}{20}, \frac{2}{15}, \frac{2}{15}, \frac{2}{15}, \frac{9}{20}\right).$$

The basis of BDM_1, φ_k and ψ_k on edge e_{ij}, are given by

$$\phi_k=\lambda_i\mathrm{curl}\,\lambda_j-\lambda_j\mathrm{curl}\,\lambda_i, \psi_k=\lambda_i\mathrm{curl}\,\lambda_j+\lambda_j\mathrm{curl}\,\lambda_i.$$

Note that $\psi_k=\frac{1}{4}\,\mathrm{curl}\,\eta_k$ and thus div $\psi_k = 0$.

As ω_b is added to the vorticity space, we add one more bubble function χ_b = curl ω_b to BDM_1 in order to ensure the inf-sup stability. After the vorticity is eliminated, the resulting scheme is denoted by $\mathrm{BDM}_1^{\mathrm{b}} - \mathrm{P}_0$.

In the implementation, the discrete differential operators are easy to construct with the hierarchical bases by using $\theta_1 = \lambda_1$, $\theta_2 = \lambda_2$, and $\theta_3 = \lambda_3$. The curl matrix from $\mathrm{P}_2^{\mathrm{b}}$ to $\mathrm{BDM}_1^{\mathrm{b}}$ will be block diagonal consisting of that from P_1 to RT_0 and one identity matrix. The curl matrix for the bases ($\hat{\theta_i}$, $\hat{\eta_i}$, ω_b) can be obtained by the transfer operator between the hierarchical bases (θ_i, η_i, ω_b) and nodal bases ($\hat{\theta_i}$, $\hat{\eta_i}$, ω_b). The non-zeros of div matrix remains the same.

3 Stability of TMAC

In this section, we prove the stability of the TMAC scheme formulation (2.8) without mass lumping and of the formulation (2.11) with mass lumping. The abstract proof works for all stable pairs $\mathrm{P_r}$–$\mathrm{RT_{r-1}}$–$\mathrm{P_{r-1}}$ and $\mathrm{P_{r+1}}$–$\mathrm{BDM_r}$–$\mathrm{P_{r-1}}$ for integer $r \geq 1$, and the stability result holds for all shape regular meshes which are not necessarily quasi-uniform.

3.1 Well-Posedness of the Discrete Formulation Without Mass Lumping

We will first prove that the bilinear form $a_h(\cdot, \cdot)$ defined in (2.7) is an inner product, and we will introduce the associated norm $\|\cdot\|_{A_h}$ on the space $\boldsymbol{V}_0^h$. Then we prove the inf-sup condition for $a_h(\cdot, \cdot)$ and $b(\cdot, \cdot)$ with respect to the norm $\|\cdot\|_{A_h}$, which implies the well-posedness of the discrete formulation (2.8).

The Hodge decomposition plays an important role in the analysis of well-posedness. On the continuous level, the Hodge (or Helmholtz) decomposition is

$$\boldsymbol{L}^2 = \mathrm{curl}\, H_0(\mathrm{curl}) \oplus \mathrm{grad}(H^1/\mathbb{R}).$$

We have an analogous discrete Hodge decomposition based on the following exact sequence:

$$\sum_0^h \xrightarrow{\mathrm{curl}} \boldsymbol{V}_0^h \xrightarrow{\mathrm{div}} S_0^h \to 0. \quad (3.1)$$

Lemma 1—(Discrete Hodge Decomposition [1]) Suppose that $\sum_0^h$, $\boldsymbol{V}_0^h$, and S_0^h are appropriate subspaces for spaces $H_0(\mathrm{curl})$, $\boldsymbol{H}_0(\mathrm{div})$, and L_0^2, respectively, such that the sequence in (3.1) is exact. Then, we have

$$\boldsymbol{V}_0^h = \mathrm{curl}\sum_0^h \oplus \mathrm{grad}_h S_0^h, \quad (3.2)$$

where the operator $grad_h$ is defined in (2.6)

Definition 3 For $\boldsymbol{u} \in \boldsymbol{V}_0^h$, define $\|\boldsymbol{u}\|_{A_h}^2 = a_h(\boldsymbol{u}, \boldsymbol{u})$.

According to the definition of $a_h(\cdot, \cdot)$ in (2.7), it is obvious that $a_h(\cdot, \cdot)$ is symmetric and semi-positive definite and thus $\|\cdot\|_{A_h}$ defines a semi-norm on $\boldsymbol{V}_0^h$. We will prove a discrete Poincaré inequality and consequently $\|\cdot\|_{A_h}$ indeed defines a norm on $\boldsymbol{V}_0^h$.

Let us first recall the following Poincaré inequalities [2]:

$$\|\phi\| \lesssim \|\mathrm{grad}_h \phi\| \text{for all } \phi \in S_0^h, \quad (3.3)$$

$$\|\rho\| \lesssim \|\mathrm{curl}\, \rho\| \text{for all } \rho \in \sum\nolimits_0^h. \quad (3.4)$$

Lemma 2—(Discrete Poincaré Inequality) We have the following discrete Poincaré inequality with respect to $\|\cdot\|_{A_h}$:

$$\|\boldsymbol{u}_h\| \lesssim \|\boldsymbol{u}_h\|_{A_h} \text{ for all } \boldsymbol{u}_h \in \boldsymbol{V}_0^h. \quad (3.5)$$

Proof From the discrete Hodge decomposition in Lemma 1, for $\boldsymbol{u}_h \in \boldsymbol{V}_0^h$, there exist $\rho \in \sum_0^h$ and $\phi \in S_0^h$ such that

$$\boldsymbol{u}_h = \mathrm{curl}\, \rho + \mathrm{grad}_h \phi. \quad (3.6)$$

By applying operator div to (3.6), we obtain div $\boldsymbol{u}_h$ = div grad$_h\varphi$. By multiplying this equation with φ, using the definition of grad$_h$ (2.6), and using (3.3), we obtain

$$\|\mathrm{grad}_h \phi\|^2 = (\mathrm{grad}_h \phi, \mathrm{grad}_h \phi) = -(\mathrm{div} \boldsymbol{u}_h, \phi) \le \|\mathrm{div} \boldsymbol{u}_h\| \|\phi\| \lesssim \|\mathrm{div} \boldsymbol{u}_h\| \|\mathrm{grad}_h \phi\|.$$

Therefore, we have $\|\mathrm{grad}_h \varphi\| \lesssim \|\ \mathrm{div}\ \boldsymbol{u}_h\|$.

For the other part, by applying rot$_h$ to $\boldsymbol{u}_h$ = curl ρ + grad$_h\varphi$ and then testing with ρ and integration by parts, we obtain

$$(\mathrm{rot}_h \boldsymbol{u}_h, \rho) = (\mathrm{rot}_h\, \mathrm{curl}\, \rho, \rho) + (\mathrm{rot}_h \mathrm{grad}_h \phi, \rho) = (\mathrm{curl}\, \rho, \mathrm{curl}\, \rho).$$

Therefore, by the Poincaré inequality for curl in (3.4), we obtain

$$\|\mathrm{curl}\, \rho\|^2 = (\mathrm{curl}\, \rho, \mathrm{curl}\, \rho) = (\mathrm{rot}_h \boldsymbol{u}_h, \rho) \le \|\mathrm{rot}_h \boldsymbol{u}_h\| \|\rho\| \lesssim \|\mathrm{curl}\, \rho\| \|\mathrm{rot}_h \boldsymbol{u}_h\|,$$

which leads to $\| \operatorname{curl} \rho\| \lesssim \|\operatorname{rot}_h \boldsymbol{u}_h\|$.

In summary, we have proved that

$$\|\boldsymbol{u}_h\| \leq \|\operatorname{curl} \rho\| + \|\operatorname{grad}_h \phi\| \lesssim \|\operatorname{rot}_h \boldsymbol{u}_h\| + \|\operatorname{div} \boldsymbol{u}_h\| \lesssim \|\boldsymbol{u}_h\|_{A_h}.$$

Remark 3 In the proof, we use the fact that for any $\phi \in S_0^h$, we have

$$(\operatorname{rot}_h \operatorname{grad}_h \phi, \rho) = (\operatorname{grad}_h \phi, \operatorname{curl} \rho) = (\phi, \operatorname{div} \operatorname{curl} \rho) = 0, \text{ for all } \rho \in \sum\nolimits_0^h. \quad (3.7)$$

However, $(\operatorname{rot}_h \operatorname{grad}_h \varphi, \rho) \neq 0$ if $\rho \in \Sigma^h$ and $\rho \notin \sum_0^h$ since now curl $\rho \notin \boldsymbol{V}_0^h$ and the second equality in (3.7) fails.

According to Lemma 2, we can obtain the following lemma, which is equivalent to the inf-sup condition of the bilinear form $a_h(\cdot, \cdot)$.

Lemma 3—The bilinear form $a_h(\cdot, \cdot)$ on $\boldsymbol{V}_0^h \times \boldsymbol{V}_0^h$ satisfies

1. Continuity: $a_h(\boldsymbol{u}, \boldsymbol{v}) \lesssim \|\boldsymbol{u}\|_{A_h} \|\boldsymbol{v}\|_{A_h}$;
2. Coercivity: $a_h(\boldsymbol{u}, \boldsymbol{u}) \gtrsim \|\boldsymbol{u}\|_{A_h}^2$.

We denote the canonical interpolations as $\prod_{\sum_0^h}: C_0(\Omega) \to \sum_0^h$, where $C_0(\Omega)$ denotes the continus functions with zero trace on $\partial\Omega$, $\prod_{\boldsymbol{V}_0^h}: \boldsymbol{H}_0(\operatorname{div}) \cap \boldsymbol{H}^1 \to \boldsymbol{V}_0^h$ and $\prod_{S_0^h}: L_0^2 \to S_0^h$. Based on P_1–RT_0–P_0 as an example, the canonical interpolations are defined as following:

$$\begin{array}{cc} \prod_{\sum_0^h}: C_0(\Omega) \to \sum_0^h, & \prod_{\sum_0^h} \rho(x_i) = \rho(x_i) \text{ for all vertices } x_i, \\ \prod_{\boldsymbol{V}_0^h}: \boldsymbol{H}_0(\operatorname{div}) \cap \boldsymbol{H}^1 \to \boldsymbol{V}_0^h, & \int_e \prod_{\boldsymbol{V}_0^h} \boldsymbol{v} \cdot \boldsymbol{n} \mathrm{d}s = \int_e \boldsymbol{v} \cdot \boldsymbol{n} \mathrm{d}s \text{ for all edges } e, \\ \prod_{S_0^h}: L_0^2 \to S_0^h, & \int_T \prod_{S_0^h} q \mathrm{d}x = \int_T q \mathrm{d}x \text{ for all triangles } T. \end{array}$$

It is well known that the canonical interpolations are commuting with the corresponding differential operators [28]. More specifically, $\operatorname{div} \prod_{\boldsymbol{V}_0^h} = \prod_{S_0^h} \operatorname{div}$ and $\operatorname{curl} \prod_{\sum_0^h} = \prod_{\boldsymbol{V}_0^h} \operatorname{curl}$.

In order to prove the inf-sup condition of the bilinear form $b(\cdot, \cdot)$ on the discrete level, we take advantage of the properties of the canonical projection; i.e., for any $\boldsymbol{v} \in \boldsymbol{H}_0^1(\Omega)$, we have $\operatorname{div} \prod_{\boldsymbol{V}_0^h} \boldsymbol{v} = \prod_{S_0^h} \operatorname{div} \boldsymbol{v}$, and $\|\boldsymbol{v} - \prod_{\boldsymbol{V}_0^h} \boldsymbol{v}\|_\tau \lesssim h_\tau \|\boldsymbol{v}\|_{1,\tau}$, where $h_\tau = \operatorname{diam}(\tau)$ and $\|\cdot\|_\tau$, $\|\cdot\|_{1,\tau}$ are norms restricted to the triangle τ.

Lemma 4—For any $q_h \in S_0^h$, there exists $\boldsymbol{v}_h \in \boldsymbol{V}_0^h$ such that

$$\operatorname{div} \boldsymbol{v}_h = q_h, \text{ and } \|\boldsymbol{v}_h\|_{A_h} \lesssim \|q_h\|.$$

Proof It is well known that the operator $\operatorname{div}: \boldsymbol{H}_0^1(\Omega) \to L_0^2$ is surjective and that the right inverse is stable [23]. Namely, for any $q_h \in S_0^h \subset L_0^2$, there exists $\boldsymbol{v} \in \boldsymbol{H}_0^1(\Omega)$ such that:

$$\operatorname{div} \boldsymbol{v} = q_h, \text{ and } \|\boldsymbol{v}\|_1 \lesssim \|q_h\|.$$

Let $\boldsymbol{v}_h = \prod_{\boldsymbol{V}_0^h} \boldsymbol{v}$, then we have $\operatorname{div} \boldsymbol{v}_h = \operatorname{div} \prod_{\boldsymbol{V}_0^h} \boldsymbol{v} = \prod_{S_0^h} \operatorname{div} \boldsymbol{v} = \prod_{S_0^h} q_h = q_h$. We prove $\|\operatorname{rot}_h \boldsymbol{v}_h\| \lesssim \|q_h\|$ as follows:

$$\begin{aligned}
&(\operatorname{rot}_h \boldsymbol{v}_h, \operatorname{rot}_h \boldsymbol{v}_h) \\
&\quad = (\operatorname{rot}_h \boldsymbol{v}_h \\
&\qquad - \operatorname{rot} \boldsymbol{v}, \operatorname{rot}_h \boldsymbol{v}_h) \\
&\quad + (\operatorname{rot} \boldsymbol{v}, \operatorname{rot}_h \boldsymbol{v}_h) \\
&\quad = (\boldsymbol{v}_h - \boldsymbol{v}, \operatorname{curl} \operatorname{rot}_h \boldsymbol{v}_h) \\
&\quad + (\operatorname{rot} \boldsymbol{v}, \operatorname{rot}_h \boldsymbol{v}_h) \lesssim \sum_{\tau \in \mathcal{T}} h_\tau^{-1} \|\boldsymbol{v} - \boldsymbol{v}_h\|_\tau \|\operatorname{rot}_h \boldsymbol{v}_h\|_\tau \\
&\quad + \|\boldsymbol{v}\|_1 \|\operatorname{rot}_h \boldsymbol{v}_h\| \lesssim \|\boldsymbol{v}\|_1 \|\operatorname{rot}_h \boldsymbol{v}_h\| \lesssim \|q_h\| \|\operatorname{rot}_h \boldsymbol{v}_h\|.
\end{aligned}$$

Then we obtain $\|\operatorname{rot}_h \boldsymbol{v}_h\| \lesssim \|q_h\|$. In summary, we have proved that $\| \boldsymbol{v}_h \|_{A_h} \lesssim \|q_h\|$.

We summarize the well-posedness of the $H(\operatorname{div})$ discretization (2.8) and the stability of the Stokes equations in the following theorem.

Theorem 1 There exists a unique solution $(\boldsymbol{u}_h, p_h) \in \boldsymbol{V}_0^h \times S_0^h$ to the weak formulation of the Stokes equations (2.8), and

$$\nu \|\boldsymbol{u}_h\|_{A_h} + \|p_h\| \lesssim \|\boldsymbol{f}\|_{A_h'},$$

Where $\|\boldsymbol{f}\|_{A_h'} = \sup_{\boldsymbol{v}_h \in \boldsymbol{V}_0^h} \frac{(\boldsymbol{f}, \boldsymbol{v}_h)}{\|\boldsymbol{v}_h\|_{A_h}}$.

Proof The existences and uniqueness is from the Babuska-Brezzi theory since the inf-sup conditions have been proved in Lemmas 3 and 4. We prove the stability as follows.

Choosing $\boldsymbol{v}_h = \boldsymbol{u}_h$ in (2.8), we obtain

$$v\|\boldsymbol{u}_h\|_{A_h}^2=(\boldsymbol{f},\boldsymbol{u}_h)\le\|\boldsymbol{f}\|_{A_h'}\|\boldsymbol{u}_h\|_{A_h},$$

which leads to the stability of $\boldsymbol{u}_h$. By Lemma 4, we can chose $\boldsymbol{v}_h\in\boldsymbol{V}_0^h$ such that div $\boldsymbol{v}_h = p_h$ and $\|\boldsymbol{v}_h\|_{A_h}\lesssim\|p_h\|$. Choosing such $\boldsymbol{v}_h$ in (2.8), we obtain

$$\|p_h\|^2=(p_h,\operatorname{div}\boldsymbol{v}_h)=(\boldsymbol{f},\boldsymbol{v}_h)-va_h(\boldsymbol{u}_h,\boldsymbol{v}_h)\le(\|\boldsymbol{f}\|_{A_h'}+v\|\boldsymbol{u}_h\|_{A_h})\|\boldsymbol{v}_h\|_{A_h}.$$

Then by the stability of $\boldsymbol{u}_h$ and the inequality $\|\boldsymbol{v}_h\|_{A_h}\lesssim\|p_h\|$, we have

$$\|p_h\|^2\lesssim\|\boldsymbol{f}\|_{A_h'}\|p_h\|,$$

which leads to the stability of p_h.

3.2 Well-Posedness of the Discrete Formulation with Mass Lumping

In this subsection, we prove the well-posedness of the discrete formulation (2.11), in which mass lumping is applied to the discrete space $\mathcal{Z}^h$. Let $\|\cdot\|_h$ denote the associated discrete L^2 norm of quadrature (2.9), i.e., $\|\rho\|_h^2=\langle\rho,\rho\rangle$. Based on the results in the previous subsection, it is sufficient to verify that the norm induced by the bilinear form $\tilde{a}_h(\cdot,\cdot)$ is equivalent to the norm $\|\cdot\|_{A_h}$.

Definition 4 For $\boldsymbol{u}\in\boldsymbol{V}_0^h$, define $\|\boldsymbol{u}\|_{\tilde{A}_h}^2=\tilde{a}_h(\boldsymbol{u},\boldsymbol{u})$.

Let us prove the following norm equivalence.

Lemma 5—Assume that the discrete L^2 norm is equivalent to the L^2 norm; i.e, $\|\rho\|_h\lesssim\|\rho\|\lesssim\|\rho\|_h$ for any $\rho\in\mathcal{Z}^h$. Then the norm $\|\cdot\|_{\tilde{A}_h}$ is equivalent to $\|\cdot\|_{A_h}$; i.e., for any $\boldsymbol{u}_h\in\boldsymbol{V}_h$,

$$\|\boldsymbol{u}_h\|_{\tilde{A}_h}\lesssim\|\boldsymbol{u}_h\|_{A_h}\lesssim\|\boldsymbol{u}_h\|_{\tilde{A}_h}.$$

Proof It suffices to prove the part associated with the operators rot_h and $\widetilde{\operatorname{rot}}_h$. By definition, we have

$$\langle\widetilde{\operatorname{rot}}_h\boldsymbol{u}_h,\tau\rangle=(\operatorname{rot}_h\boldsymbol{u}_h,\tau)=(\boldsymbol{u}_h,\operatorname{curl}\tau)\text{ for all }\tau\in\sum{}^h. \quad (3.8)$$

Let $\tau=\widetilde{\mathrm{rot}}_h \boldsymbol{u}_h$ in (3.8), and use $\|\widetilde{\mathrm{rot}}_h \boldsymbol{u}_h\|_h \lesssim \|\widetilde{\mathrm{rot}}_h \boldsymbol{u}_h\| \lesssim \|\widetilde{\mathrm{rot}}_h \boldsymbol{u}_h\|_h$ to get $\|\widetilde{\mathrm{rot}}_h \boldsymbol{u}_h\|_h^2=\langle\widetilde{\mathrm{rot}}_h \boldsymbol{u}_h, \widetilde{\mathrm{rot}}_h \boldsymbol{u}_h\rangle=(\mathrm{rot}_h \boldsymbol{u}_h, \widetilde{\mathrm{rot}}_h \boldsymbol{u}_h) \leq \|\mathrm{rot}_h \boldsymbol{u}_h\|\|\widetilde{\mathrm{rot}}_h \boldsymbol{u}_h\| \lesssim \|\mathrm{rot}_h \boldsymbol{u}_h\|\|\widetilde{\mathrm{rot}}_h \boldsymbol{u}_h\|_h$, which leads to $\|\boldsymbol{u}_h\|_{\tilde{A}_h} \lesssim \|\boldsymbol{u}_h\|_{A_h}$. The other inequality can be proved similarly.

By Lemma 5, the stability results of the bilinear forms $\tilde{a}_h(\cdot, \cdot)$ and $b(\cdot, \cdot)$ with respect to the norm $\|\cdot\|_{\tilde{A}_h}$ are straightforward. Thus, we have proved the well-posedness of the $H(\mathrm{div})$ discretization (2.11) of the Stokes equations.

Theorem 2 Assume that the discrete L^2 norm is equivalent to the L^2 norm. Then there exists a unique solution $(\boldsymbol{u}_h, p_h) \in \boldsymbol{V}_0^h \times S_0^h$ to the weak formulation of the Stokes equations (2.11) and

$$v\|\boldsymbol{u}_h\|_{\tilde{A}_h}+\|p_h\| \lesssim \|\boldsymbol{f}\|_{\tilde{A}_h'},$$

Where $\|\boldsymbol{f}\|_{\tilde{A}_h'} = \sup_{\boldsymbol{v}_h \in \boldsymbol{V}_0^h} \frac{(\boldsymbol{f}, \boldsymbol{v}_h)}{\|\boldsymbol{v}_h\|_{\tilde{A}_h}}$.

In particular, for the two mass lumping schemes considered in this paper, the corresponding discrete L^2 norm is equivalent to the L^2 norm and thus the corresponding discretization is stable.

4 Error Analysis

In this section, we prove that for the RT_0–P_0 approximation, the convergence order depends on the symmetry of the mesh. For the BDM_1–P_0 approximation, first-order convergence is always achieved. The results in this section are derived for quasi-uniform meshes $\mathcal{T}_h$ for which all triangles are shape regular and of comparable diameter h.

Let us clarify the notation before we present the details of our error analysis. For a given space pair $(\sum^h, \boldsymbol{V}_0^h, S_0^h)$, let $(\omega_\mathrm{I}, \boldsymbol{u}_\mathrm{I}, p_\mathrm{I})$ denote the canonical interpolation of $(\omega, \boldsymbol{u}, p)$; i.e., $\omega_\mathrm{I}=\prod_{\sum^h}\omega, \boldsymbol{u}_\mathrm{I}=\prod_{\boldsymbol{V}_0^h}\boldsymbol{u}$ and $p_\mathrm{I}=\prod_{S_0^h} p$, and $(\omega_h, \boldsymbol{u}_h, p_h)$ denote the numerical solution of (2.8). For vorticity ω, the approximation without mass lumping is denoted by $\omega_h = \mathrm{rot}_h \boldsymbol{u}_h$, and the approximation with mass lumping by $\tilde{\omega}_h=\tilde{\mathrm{rot}}_h \boldsymbol{u}_h$. The choice of spaces $(\sum^h, \boldsymbol{V}_0^h, S_0^h)$ will be indicated in the context. For an integer $r \geq 1$, we will use $\sum_r^h$ to indicate the degree of polynomial used for the Lagrange element is r.

In the proof, we will use the L^2 projection $Q_h : L^2 \to \Sigma^h$ which is defined such that for a given $f \in L^2$, $Q_h f \in \Sigma^h$ satisfies

$$(Q_h f, \tau_h)=(f, \tau_h) \text{ for all } \tau_h \in \sum^h.$$

The following approximation properties of the L^2 projection are well known.

Lemma 6—For any quasi-uniform mesh with mesh size h, the L^2 projection $Q_h: L^2 \to \sum_r^h$ satisfies

$$\|\phi - Q_h\phi\| + h|\phi - Q_h\phi|_1 \lesssim h^s|\phi|_s \text{ for all } \phi \in H^s,$$

where $1 \le s \le r$.

4.1 Error Analysis of the RT_0–P_0 Formulation Without Mass Lumping

First we present a definition for the irregular triangulation following Bank and Xu [4]. We also recall their superconvergence result. Based on that, we obtain the error estimates for both velocity and pressure, each of which has an optimal order on meshes with certain symmetry.

Let e be an interior edge in the triangulation $\mathcal{T}_h$. Let τ and τ' be the two triangles sharing e. We say that τ and τ' form an $\mathcal{O}(h^2)$ approximate parallelogram if the lengths of any two opposite edges differ only by $\mathcal{O}(h^2)$. Let x be a vertex lying on $\partial\Omega$, and let e and e' be the two boundary edges sharing x as an endpoint. Let τ and τ' be the two elements having e and e', respectively, as edges, and let $\boldsymbol{t}$ and $\boldsymbol{t}'$ be the unit tangents of e and e', respectively. Take e and e' as one pair of corresponding edges, and make a clockwise traversal of $\partial\tau$ and $\partial\tau'$ to define two additional corresponding edge pairs. In this case, we say that τ and τ' form an $\mathcal{O}(h^2)$ approximate parallelogram if $|\boldsymbol{t} - \boldsymbol{t}'| = \mathcal{O}(h)$, and the lengths or any two corresponding edges differ only by $\mathcal{O}(h^2)$.

Definition 5 Given a triangulation $\mathcal{T}_h$, the triangulation $\mathcal{T}_h$ is $\mathcal{O}(h^{2\sigma})$ irregular if the following hold:

- **a.** Let $\varepsilon = \varepsilon_1 \oplus \varepsilon_2$ denote the set of interior edges in the triangulation mesh. For any $e \in \varepsilon_1$, two triangles τ_e and τ_e' containing e form an $\mathcal{O}(h^2)$ approximate parallelogram, and $\sum_{e\in\varepsilon_2} |\tau_e| + |\tau_e'| = \mathcal{O}(h^{2\sigma})$.
- **b.** Let $= \mathcal{P} = \mathcal{P}_1 \oplus \mathcal{P}_2$ denote the set of boundary vertices. The elements associated with each $x \in \mathcal{P}_1$ form an $\mathcal{O}(h^2)$ approximate parallelogram, and $|\mathcal{P}_2| = \kappa$ where κ is independent of h.

Examples of $\mathcal{O}(h^{2\sigma})$ irregular grids can be found in Sect. 5.

Remark 4 It is straightforward to generalize our error analysis to the mesh in which an $\mathcal{O}(h^{1+\alpha})$ approximated parallelogram property holds for most pairs of triangles [31,49]. For such meshes, the rate $\min(1, \sigma)$ will be replaced by $\min(\alpha, \sigma)$.

Lemma 7—(Bank and Xu [4]) Assume that $\rho \in W^{3,\infty} \cap H_0^1$ and that the triangulation $\mathcal{T}_h$ is $\mathcal{O}(h^{2\sigma})$. Let ρ_I be the piecewise linear nodal interpolation of ρ based on $\mathcal{T}_h$. Then for any continuous and piecewise linear function ϕ_h,

$$|(\nabla(\rho-\rho_{\mathrm{I}}),\nabla_{\varphi_h})|\lesssim h^{1+\min(1,\sigma)}|\log h|^{1/2}\|\rho\|_{3,\infty,\Omega}|\varphi_h|_{1,\Omega}. \quad (4.1)$$

First, we give an estimate of the interpolation operator with the help of Lemmas 6 and 7. In making this estimate, we draw on [3] and note that the general consistency analysis on the codifferential operators can be found in [3].

Lemma 8—Assume that $\boldsymbol{u}\in\boldsymbol{W}^{2,\infty}\cap\boldsymbol{H}_0^1$, div **u** = 0, and the triangulation is $\mathcal{O}(h^{2\sigma})$ irregular. For the RT_0 space, we have the interpolation error estimate

$$\|\mathrm{rot}\,\boldsymbol{u}-\mathrm{rot}_h\boldsymbol{u}_{\mathrm{I}}\|\lesssim h^{\min(1,\sigma)}|\log h|^{1/2}\|\boldsymbol{u}\|_{2,\infty}.$$

Proof By the triangle inequality and the first-order approximation of Q_h in the L^2 norm in Lemma 6, we have

$$\|\mathrm{rot}\,\boldsymbol{u}-\mathrm{rot}_h\boldsymbol{u}_{\mathrm{I}}\|\le\|\mathrm{rot}\,\boldsymbol{u}-Q_h\mathrm{rot}\,\boldsymbol{u}\|+\|Q_h\mathrm{rot}\,\boldsymbol{u}-\mathrm{rot}_h\boldsymbol{u}_{\mathrm{I}}\|\lesssim h|\mathrm{rot}\,\boldsymbol{u}|_1+\|Q_h\mathrm{rot}\,\boldsymbol{u}-\mathrm{rot}_h\boldsymbol{u}_{\mathrm{I}}\|.$$

Let us estimate the second term. As div $\boldsymbol{u}$ = 0 and $\boldsymbol{u}\in\boldsymbol{W}^{2,\infty}\cap\boldsymbol{H}_0^1$, there exists a $\rho\in W^{3,\infty}\bigcap H_0(\mathrm{curl})$ such that $\boldsymbol{u}$ = curl ρ. As the canonical projections commute with differential operators, we have $\boldsymbol{u}_{\mathrm{I}}=\prod_{V_0^h}\boldsymbol{u}=\prod_{V_0^h}\mathrm{curl}\,\rho=\mathrm{curl}\prod_{\sum_0^h}\rho=\mathrm{curl}\,\rho_I$. For any $q_h\in\Sigma^h$, we have

$$\begin{aligned}&(Q_h\mathrm{rot}\,\boldsymbol{u}-\mathrm{rot}_h\boldsymbol{u}_{\mathrm{I}},q_h)\\&\quad=(\mathrm{rot}\,\boldsymbol{u}-\mathrm{rot}_h\boldsymbol{u}_{\mathrm{I}},q_h)\\&\quad=(\boldsymbol{u}-\boldsymbol{u}_{\mathrm{I}},\mathrm{curl}\,q_h)=(\mathrm{curl}\,\rho-\mathrm{curl}_{\rho_I},\mathrm{curl}_{q_h})\\&\quad=(\nabla(\rho\\&\qquad-\rho_I),\nabla_{q_h})\lesssim h^{1+\min(1,\sigma)}|\log h|^{1/2}\|\rho\|_{3,\infty}|q_h|_1\lesssim h^{\min(1,\sigma)}|\log h|^{1/2}\|\boldsymbol{u}\|_{2,\infty}\|q_h\|.\end{aligned}$$

Thus, we have $\|Q_h\,\mathrm{rot}\,\boldsymbol{u}-\mathrm{rot}_h\boldsymbol{u}_{\mathrm{I}}\|\lesssim h^{\min(1,\sigma)}\,|\log\,h|^{1/2}\|\boldsymbol{u}\|_{2,\infty}$, such that the desired estimate is obtained.

Then, we present the convergence result for the RT_0−P_0 discretization.

Theorem 3 Assume that the solution of the Stokes equations satisfies $\boldsymbol{u}\in\boldsymbol{W}^{2,\infty}\cap\boldsymbol{H}_0^1$ and rot $\boldsymbol{u}\in\boldsymbol{H}^2$. Assume the triangulation mesh is $\mathcal{O}(h^{2\sigma})$ irregular. Let $\boldsymbol{u}_{\mathrm{h}}$ and p_h be the solution of the RT_0−P_0 approximation using formulation (2.8). Then, we have the error estimate

$$\|\omega-\omega_h\|+\|\boldsymbol{u}_h-\boldsymbol{u}_{\mathrm{I}}\|_{A_h}+\nu^{-1}\|p_h-p_{\mathrm{I}}\|\lesssim h^{\min(1,\sigma)}|\log h|^{1/2}(\|\boldsymbol{u}\|_{2,\infty}+\|\mathrm{rot}\,\boldsymbol{u}\|_2).$$

Proof Notice that div $\boldsymbol{u}_h = 0$ and $\operatorname{div} \boldsymbol{u}_{\mathrm{I}} = \operatorname{div} \prod_{\boldsymbol{V}_0^h} \boldsymbol{u} = \prod_{S_0^h} \operatorname{div} \boldsymbol{u} = 0$. It is evident that

$$\begin{aligned}
&a_h(\boldsymbol{u}_h - \boldsymbol{u}_{\mathrm{I}}, \boldsymbol{v}_h) \\
&\quad = \boldsymbol{v}^{-1}(\boldsymbol{f}, \boldsymbol{v}_h) \\
&\quad + \boldsymbol{v}^{-1}(p_h, \operatorname{div} \boldsymbol{v}_h) - (\operatorname{rot}_h \boldsymbol{u}_{\mathrm{I}}, \operatorname{rot}_h \boldsymbol{v}_h) \\
&\quad = (\operatorname{curl} \ \operatorname{rot} \boldsymbol{u}, \boldsymbol{v}_h) \\
&\quad - (\operatorname{rot}_h \boldsymbol{u}_{\mathrm{I}}, \operatorname{rot}_h \boldsymbol{v}_h) \\
&\quad - \boldsymbol{v}^{-1}(p \\
&\qquad - p_h, \operatorname{div} \boldsymbol{v}_h) = (\operatorname{rot} \boldsymbol{u} - \operatorname{rot}_h \boldsymbol{u}_I, \operatorname{rot}_h \boldsymbol{v}_h) \\
&\quad + (\operatorname{curl}(I \\
&\qquad - Q_h) \operatorname{rot} \boldsymbol{u}, \boldsymbol{v}_h) \\
&\quad + v^{-1}(p \\
&\qquad - p_h, -\operatorname{div} \boldsymbol{v}_h): \\
&\quad = I_1 + I_2 + I_3.
\end{aligned}$$

By Lemma 8, we can obtain the error estimate of the first part:

$$I_1 = (\operatorname{rot} \boldsymbol{u} - \operatorname{rot}_h \boldsymbol{u}_{\mathrm{I}}, \operatorname{rot}_h \boldsymbol{v}_h) \leq \|\operatorname{rot} \boldsymbol{u} - \operatorname{rot}_h \boldsymbol{u}_{\mathrm{I}}\| \|\operatorname{rot}_h \boldsymbol{v}_h\| \lesssim h^{\min(1,\sigma)} |\log h|^{1/2} \|\boldsymbol{u}\|_{2,\infty} \|\boldsymbol{v}_h\|_{A_h}.$$

Using the first-order approximation of the L^2 projection Q_h in the H^1 norm in Lemma 6, we have

$$I_2 = (\operatorname{curl}(I - Q_h) \operatorname{rot} \boldsymbol{u}, \boldsymbol{v}_h) \leq \|\operatorname{curl}(I - Q_h) \operatorname{rot} \boldsymbol{u}\| \|\boldsymbol{V}_h\| \lesssim h \|\operatorname{rot} \boldsymbol{u}\|_2 \|\boldsymbol{v}_h\|_{A_h}.$$

If we choose $\boldsymbol{v}_h = \boldsymbol{u}_I - \boldsymbol{u}_h$, it is easy to see that $I_3 = \nu^{-1}(p - p_h, -\operatorname{div} \boldsymbol{v}_h) = 0$. By combining these estimates, we obtain

$$\|\boldsymbol{u}_h - \boldsymbol{u}_{\mathrm{I}}\|_{A_h}^2 \lesssim h^{\min(1,\sigma)} |\log h|^{1/2} (\|\boldsymbol{u}\|_{2,\infty} + \|\operatorname{rot} \boldsymbol{u}\|_2) \|\boldsymbol{u}_h - \boldsymbol{u}_{\mathrm{I}}\|_{A_h},$$

which leads to the estimate of $\|\boldsymbol{u}_h - \boldsymbol{u}_I\|_{A_h}$.

By Lemma 8 and the error estimate of the velocity, we obtain

$$\|\omega - \omega_h\| \leq \|\operatorname{rot} \boldsymbol{u} - \operatorname{rot}_h \boldsymbol{u}_{\mathrm{I}}\| + \|\operatorname{rot}_h \boldsymbol{u}_{\mathrm{I}} - \operatorname{rot}_h \boldsymbol{u}_h\| \lesssim h^{\min(1,\sigma)} |\log h|^{1/2} (\|\boldsymbol{u}\|_{2,\infty} + \|\operatorname{rot} \boldsymbol{u}\|_2).$$

To prove the error estimate of the pressure, for any $\boldsymbol{v}_h \in \boldsymbol{v}_0^h$, we have

$$\boldsymbol{v}^{-1}b(p_{\mathrm{I}}-p_h,\boldsymbol{v}_h)=\boldsymbol{v}^{-1}b(p_{\mathrm{I}},\boldsymbol{v}_h)+a_h(\boldsymbol{u}_h,\boldsymbol{v}_h)-\boldsymbol{v}^{-1}(\boldsymbol{f},\boldsymbol{v}_h)=[a_h(\boldsymbol{u}_h,\boldsymbol{v}_h)-(\mathrm{curl}\ \ \mathrm{rot}\,\boldsymbol{u},\boldsymbol{v}_h)]+v^{-1}b(p_{\mathrm{I}}-p,\boldsymbol{v}_h):=I_4+I_5.$$

By the stability result presented in Lemma 4, we can choose $\boldsymbol{v}_h \in \boldsymbol{V}_0^h$ such that

$$\mathrm{div}\,\boldsymbol{v}_h=p_{\mathrm{I}}-p_h,\ \text{and}\ \|\boldsymbol{v}_h\|_{A_h}\lesssim\|p_{\mathrm{I}}-p_h\|.$$

With such $\boldsymbol{v}_h$, we have

$$\begin{aligned}I_4=&a_h(\boldsymbol{u}_h,\boldsymbol{v}_h)\\&-(\mathrm{curl}\ \ \mathrm{rot}\,\boldsymbol{u},\boldsymbol{v}_h)\\&=[(\mathrm{rot}_h\boldsymbol{u}_h,\mathrm{rot}_h\boldsymbol{v}_h)-(\mathrm{rot}\,\boldsymbol{u},\mathrm{rot}_h\boldsymbol{v}_h)]+)\mathrm{curl}\,Q_h-I)\mathrm{rot}\,\boldsymbol{u},\boldsymbol{v}_h\\=&(\omega_h-\omega,\mathrm{rot}_h\boldsymbol{v}_h)\\&-I_2\le\|\omega\\&-\omega_h\|\|\boldsymbol{v}_h\|_{A_h}\\&+h\|\mathrm{rot}\,\boldsymbol{u}\|_2\|\boldsymbol{v}_h\|_{A_h}\lesssim h^{(\min 1,\sigma)}|\log h|^{1/2}(\|\boldsymbol{u}\|_{2,\infty}\\&+\|\mathrm{rot}\,\boldsymbol{u}\|_2)\|p_{\mathrm{I}}-p_h\|.\end{aligned}$$

For part I_5, since p_{I} is the L^2 projection of p to S_0^h space,

$$I_5=v^{-1}b(p_{\mathrm{I}}-p,\boldsymbol{v}_h)=(p_{\mathrm{I}}-p,\mathrm{div}\,\boldsymbol{v}_h)=0.$$

Overall, we obtain

$$v^{-1}\|p_{\mathrm{I}}-p_h\|^2=b(p_{\mathrm{I}}-p_h,\boldsymbol{v}_h)\lesssim h^{\min(1,\sigma)}|\log h|^{1/2}(\|\boldsymbol{u}\|_{2,\infty}+\|\mathrm{rot}\,\boldsymbol{u}\|_2)\|p_{\mathrm{I}}-p_h\|.$$

By dividing $\|p_{\mathrm{I}}-p_h\|$ on both sides, we obtain the desired estimate.

Remark 5 The term $I_3 = v^{-1}(p - p_h, -\mathrm{div}\,\boldsymbol{u}_h)$ vanishes due to the point-wise divergence free of the velocity. For weakly divergence free elements, in general $(p, \mathrm{div}\,\boldsymbol{u}_h) \neq 0$ and therefore the right-hand side of the error estimate will involve the term $v^{-1}\|p - p_I\|$ which might be large when the pressure gradient is large or v is small (i.e. the Reynolds number is large). Our error estimate of the velocity and the vorticity is independent of pressure and v. Thus our schemes can produce more accurate and robust approximation of the velocity and the vorticity.

Remark 6 Let x_τ denote the barycenter of a triangle τ. We define the interpolation operator $I_h : C(\Omega) \to S^h$ as

$$I_h p(x_\tau) = p(x_\tau) \text{ for all } \tau \in \mathcal{T}_h.$$

As both the L^2 projection and interpolation I_h preserve piecewise constant functions, if $p \in H^1 \cap L_0^2 \cap C(\Omega$, then

$$\|p_1 - I_h p\| \lesssim h|p|_1.$$

For the pressure error estimate in Theorem 3, we can obtain the same order of convergence for an H^1 pressure if we replace the L^2 projection p_I with the interpolation $I_h p$.

4.2 Error Analysis of RT_0–P_0 Formulation with Mass Lumping

In this subsection, we prove the error estimates of element RT_0–P_0 with mass lumping.

Define the discrete L^2 projection with mass lumping $\tilde{Q_h}: L^2 \to \Sigma^h$, as for any $f \in L^2$

$$\left\langle \tilde{Q}_h f, \tau \right\rangle = (f, \tau) \text{ for all } \tau \in \sum^h.$$

The following first-order approximation of $\tilde{Q_h}$ in the L^2 norm is crucial to ensuring the approximation of mass lumping.

Lemma 9—For any quasi-uniform triangulation with size h, the discrete L^2 projection $\tilde{Q}_h: L^2 \to \sum_1^h$ satisfies

$$\|\phi - \tilde{Q}_h \phi\| \lesssim h|\phi|_1, \ for\ all \phi \in H^1.$$

Proof Let $\{\lambda_i, i = 1, \ldots, N\}$ denote the nodal bases of $\mathcal{L}^h$. By the definition of $\tilde{Q_h}$ and by $\sum_{i=1}^N \lambda_i(x) = 1$, we have $\phi(x) = \sum_{i=1}^N \lambda_i(x)\phi(x)$ and $\tilde{Q}_h\phi(x) = \sum_{i=1}^N \frac{(\phi, \lambda_i)}{\int_\Omega \lambda_i dx}\lambda_i(x)$, then we get

$$\|\phi - \tilde{Q}_h \phi\| = \|\sum_{i=1}^N \left[\phi\lambda_i - \frac{(\phi, \lambda_i)}{\int_\Omega \lambda_i dx}\lambda_i\right]\| \lesssim \sum_{i=1}^N \|\phi - \frac{(\phi, \lambda_i)}{\int_\Omega \lambda_i dx}\|_{\Omega_i} \lesssim h|\phi|_1.$$

Here, in the last step, we use the fact that the functional $\phi - \frac{(\phi, \lambda_i)}{\int_\Omega \lambda_i dx}$ preserves the piecewise constant function on Ω_i, where Ω_i is the support of the i-th basis function λ_i.

Lemma 10—Assume that $\boldsymbol{u} \in \boldsymbol{W}^{2,\infty} \cap \boldsymbol{H}_0^1$, div $\boldsymbol{u}$ = 0 and that the triangulation mesh is $\mathcal{O}(h^{2\sigma})$ irregular. Let $\boldsymbol{u}_I$ be the canonical interpolation of $\boldsymbol{u}$ on to RT_0. Then, we have the error estimate

$$\|\mathrm{rot}\,\boldsymbol{u} - \tilde{\mathrm{rot}}_h \boldsymbol{u}_I\| \lesssim h^{\min(1,\sigma)} |\log h|^{1/2} \|\boldsymbol{u}\|_{2,\infty}.$$

Proof Using $Q\tilde{h}$ to replace Q_h in the proof of Lemma 8, we have

$$\|\mathrm{rot}\,\boldsymbol{u} - \mathrm{rot}_h \boldsymbol{u}_I\| \le \|\mathrm{rot}\,\boldsymbol{u} - \tilde{Q}_h \mathrm{rot}\,\boldsymbol{u}\| + \|\tilde{Q}_h \mathrm{rot}\,\boldsymbol{u} - \tilde{\mathrm{rot}}_h \boldsymbol{u}_I\| \lesssim h|\mathrm{rot}\,\boldsymbol{u}|_1 + \|\tilde{Q}_h \mathrm{rot}\,\boldsymbol{u} - \tilde{\mathrm{rot}}_h \boldsymbol{u}_I\|_h.$$

To estimate the second term, we test with a $q_h \in \Sigma^h$:

$$\left\langle \tilde{Q}_h \mathrm{rot}\,\boldsymbol{u} - \tilde{\mathrm{rot}}_h \boldsymbol{u}_I, q_h \right\rangle = (\mathrm{rot}\,\boldsymbol{u} - \mathrm{rot}_h \boldsymbol{u}_I, q_h) = (\boldsymbol{u} - \boldsymbol{u}_I, \mathrm{curl}\, q_h).$$

The rest is the same as the proof of Lemma 8.

Theorem 4 Assume that the solution of the Stokes equations satisfies $\boldsymbol{u} \in \boldsymbol{W}^{2,\infty} \cap \boldsymbol{H}_0^1$ and rot $\boldsymbol{u} \in \boldsymbol{H}^2$, and that the triangulation mesh is $\mathcal{O}(h^{2\sigma})$ irregular. Let $\boldsymbol{u}_h$ and p_h be the solution of the RT_0−P_0 approximation using formulation (2.11). Then, we have the error estimate

$$\|\omega - \tilde{\omega}_h\| + \|\boldsymbol{u} - \boldsymbol{u}_I\|_{\tilde{A}h} + v^{-1}\|p_h - p_I\| \lesssim h^{\min(1,\sigma)} |\log h|^{1/2} (\|\boldsymbol{u}\|_{2,\infty} + \|\mathrm{rot}\,\boldsymbol{u}\|_2).$$

Proof Similar to the proof of Theorem 3, we have

$$\begin{aligned}
&\tilde{a}_h(\boldsymbol{u}_h - \boldsymbol{u}_I, \boldsymbol{v}_h) \\
&\quad = (\mathrm{rot}\,\boldsymbol{u} - \tilde{\mathrm{rot}}_h \boldsymbol{u}_1, \tilde{\mathrm{rot}}_h \boldsymbol{v}_h) \\
&\quad + (\mathrm{curl}(I \\
&\qquad - \tilde{Q}_h)\mathrm{rot}\,\boldsymbol{u}, \boldsymbol{v}_h) \\
&\quad + v^{-1}(p \\
&\qquad - p_h, -\mathrm{div}\,\boldsymbol{v}_h) = (\mathrm{rot}\,\boldsymbol{u} - \tilde{\mathrm{rot}}_h \boldsymbol{u}_I, \tilde{\mathrm{rot}}_h \boldsymbol{v}_h) \\
&\quad + (\mathrm{curl}(I \\
&\qquad - Q_h)\mathrm{rot}\,\boldsymbol{u}, \boldsymbol{v}_h) \\
&\quad + v^{-1}(p \\
&\quad - p_h, -\mathrm{div}\,\boldsymbol{v}_h) + (\mathrm{curl}(Q_h \\
&\qquad - \tilde{Q}_h)\mathrm{rot}\,\boldsymbol{u}, \boldsymbol{v}_h): \\
&\quad = I_1 + I_2 + I_3 + I_4.
\end{aligned}$$

The error estimates of the first three terms were obtained in Lemma 10 and Theorem 3. For the last term, we obtain the following estimate by using the first-order approximation of Q_h and Q_h~ in the L^2 norm,

$$I_4=(\mathrm{curl}(Q_h-\tilde{Q}_h)\mathrm{rot}\,\boldsymbol{u},\boldsymbol{v}_h)=((Q_h-\tilde{Q}_h)\mathrm{rot}\,\boldsymbol{u},\mathrm{rot}_h\boldsymbol{v}_h)\lesssim h|\mathrm{rot}\,\boldsymbol{u}|_1\|\boldsymbol{v}_h\|_{\tilde{A}h}.$$

As with the proof of Theorem 3, we can finish the error estimate and obtain the desired results.

4.3 Error Analysis of the RT_0−P_0 Formulation on General Unstructured Grids

The error estimate in Theorem 4 relies on the symmetry of the edge patch through the parameter σ. For general grids with $\sigma = 0$, there is no order due to the inconsistency of the interpolation. In this subsection, we obtain error estimates for the discrete formulation (2.8) with the RT_0−P_0 element on the general unstructured grids by taking advantage of the projection operator constructed in [2].

Definition 6 (Arnold et al. [2]) Define the projection operator $P_{V_0^h}:\boldsymbol{H}_0(\mathrm{div})\to\boldsymbol{V}_0^h, P_{V_0^h}\boldsymbol{v}=\boldsymbol{v}_{\mathrm{II}}$ by the equation

$$(\boldsymbol{v}_{\mathrm{II}},\mathrm{curl}\,\tau+\mathrm{grad}_h s)=(\boldsymbol{v},\mathrm{curl}\,\tau)-(\mathrm{div}\,\boldsymbol{v},s)\ \text{for all}\ \tau\in\sum_0^h, s\in S^h. \quad (4.2)$$

The estimate of the projection operator is given in the following lemma.

Lemma 11—(Arnold et al. [2]) Let $\boldsymbol{v}_{\mathrm{II}}$ be the projection of $\boldsymbol{v}$ on to RT_0 in Definition 6. Then, for any quasi-uniform triangulation with size h,

$$(\boldsymbol{v}-\boldsymbol{v}_{\mathrm{II}},\mathrm{curl}\,\tau)\lesssim h^{1/2}|\log h|\|\boldsymbol{v}\|_{1,\infty}\|\tau\| for\ all \boldsymbol{v}\in W^{1,\infty},\tau\in\sum{}^h.$$

Lemma 12—Assume that $\boldsymbol{u}\in\boldsymbol{W}^{1,\infty}\cap\boldsymbol{H}_0^1$ and rot $\boldsymbol{u}\in\boldsymbol{H}^1$. Let $\boldsymbol{u}_{\mathrm{II}}$ be the projection of $\boldsymbol{v}$ on to RT_0 in Definition 6. Then, we have the error estimate

$$\|\mathrm{rot}\,\boldsymbol{u}-\mathrm{rot}_h\boldsymbol{u}_{\mathrm{II}}\|\lesssim h^{1/2}(|\log h|\|\boldsymbol{u}\|_{1,\infty}+h^{1/2}|\mathrm{rot}\,\boldsymbol{u}|_1).$$

Proof By the triangle inequality, we have

$$\|\mathrm{rot}\,\boldsymbol{u}-\mathrm{rot}_h\boldsymbol{u}_{\mathrm{II}}\|\le\|\mathrm{rot}\,\boldsymbol{u}-Q_h\mathrm{rot}\,\boldsymbol{u}\|+\|Q_h\mathrm{rot}\,\boldsymbol{u}-\mathrm{rot}_h\boldsymbol{u}_{\mathrm{II}}\|\lesssim h|\mathrm{rot}\,\boldsymbol{u}|_1+\|Q_h\mathrm{rot}\,\boldsymbol{u}-\mathrm{rot}_h\boldsymbol{u}_{\mathrm{II}}\|.$$

To estimate the second term, we have for any $q_h\in\Sigma^h$,

$$(Q_h\mathrm{rot}\,\boldsymbol{u}-\mathrm{rot}_h\boldsymbol{u}_{\mathrm{II}},q_h)=(\mathrm{rot}\,\boldsymbol{u}-\mathrm{rot}_h\boldsymbol{u}_{\mathrm{II}},q_h)=(\boldsymbol{u}-\boldsymbol{u}_{\mathrm{II}},\mathrm{curl}\,q_h)\lesssim h^{1/2}|\log h|\|\boldsymbol{u}\|_{1,\infty}\|q_h\|.$$

Thus, we have $\|Q_h\ \mathrm{rot}\ \boldsymbol{u}-\mathrm{rot}_h\ \boldsymbol{u}_{\mathrm{II}}\|\lesssim h^{1/2}\ |\log h|\|\boldsymbol{u}\|_{1,\infty}$ and thereby obtain the desired estimate.

Similarly, the error estimates for the velocity, the vorticity, and the pressure on general unstructured grids can be obtained by following the proof of Theorem 3.

Theorem 5 (Arnold et al. [2]) Assume that the solution of the Stokes equations satisfies $\boldsymbol{u}\in\boldsymbol{W}^{1,\infty}\cap\boldsymbol{H}_0^1$ and rot $\boldsymbol{u}\in\boldsymbol{H}^2$. Let $\boldsymbol{u}_h$ and p_h be the solution of the $\mathrm{RT}_0-\mathrm{P}_0$ approximation using formulation (2.8). Then, we have the following error estimate

$$\|\omega-\omega_h\|+\|\boldsymbol{u}_h-\boldsymbol{u}_{\mathrm{II}}\|_{A_h}+v^{-1}\|p_h-p_{\mathrm{I}}\|\lesssim h^{1/2}(|\log h|\|\boldsymbol{u}\|_{1,\infty}+h^{1/2}\|\mathrm{rot}\,\boldsymbol{u}\|_2).$$

Remark 7 The error estimates of Lemma 12 and Theorem 5 can easily be generalized to the lumped case formulation (2.11) according to the analysis of Subsect. 4.2.

Remark 8 Compared with Theorem 3 for general unstructured grids with $\sigma<\frac{1}{2}$, the error estimates in Theorem 5 increase from order σ to $\frac{1}{2}$. However, for grids with $\sigma>\frac{1}{2}$, we can obtain better error estimates by Theorems 3 and 4.

4.4 Error Analysis of the BDM_1–P_0 Formulation Without Mass Lumping

In this subsection, we present the error estimates for the discrete formulation (2.8) with the BDM_1–P_0 element. The first-order convergence for the velocity and the pressure is obtained without any constraint on the irregularity of meshes.

Lemma 13—Assume that $\boldsymbol{u}\in\boldsymbol{H}^2\cap\boldsymbol{H}_0^1$, and div $\boldsymbol{u}=0$. Let $\boldsymbol{u}_{\mathrm{I}}$ be the canonical interpolation of $\boldsymbol{u}$ on to BDM_1. Then, we have the error estimate

$$\|\mathrm{rot}\,\boldsymbol{u}-\mathrm{rot}_h\boldsymbol{u}_{\mathrm{I}}\|\lesssim h\|\boldsymbol{u}\|_2.$$

Proof As in Lemma 8, we have $\|\mathrm{rot}\ \boldsymbol{u}-\mathrm{rot}_h\boldsymbol{u}_{\mathrm{I}}\|\lesssim h\|\mathrm{rot}\ \boldsymbol{u}\|_1+\|Q_h\ \mathrm{rot}\ \boldsymbol{u}-\mathrm{rot}_h\boldsymbol{u}_{\mathrm{I}}\|$.

In regard estimating the second term, the only difference to the proof of Lemma 8 is that $\rho_{\mathrm{I}}\in\mathrm{P}_2$. Thus, we have

$$(\boldsymbol{Q}_h\mathrm{rot}\,\boldsymbol{u}-\mathrm{rot}_h\boldsymbol{u}_{\mathrm{I}},q_h)=(\nabla(\rho-\rho_I),\nabla q_h)\lesssim h^2\|\rho\|_3|q_h|_1\lesssim h\|\boldsymbol{u}\|_2\|q_h\|.$$

As $\|\mathrm{rot}\ \boldsymbol{u}\|_1\le\|\boldsymbol{u}\|_2$, we obtain $\|\mathrm{rot}\ \boldsymbol{u}-\mathrm{rot}_h\boldsymbol{u}_{\mathrm{I}}\|\lesssim h\|\boldsymbol{u}\|_2$.

The following result can be proved using the proof of Theorem 3 and the improved interpolation error estimate in Lemma 13.

Theorem 6 Assume that the solution of the Stokes equations satisfies $\boldsymbol{u} \in \boldsymbol{H}^2 \cap \boldsymbol{H}_0^1$ and rot $\boldsymbol{u} \in H^2$. Let $\boldsymbol{u}_h$ and p_h be the solution of the BDM_1–P_0 approximation using formulation (2.8). Then, we have the following error estimate

$$\|\omega - \omega_h\| + \|\boldsymbol{u}_h - \boldsymbol{u}_{\mathrm{I}}\|_{A_h} + v^{-1}\|p_h - p_{\mathrm{I}}\| \lesssim h(\|\boldsymbol{u}\|_2 + \|\mathrm{rot}\, \boldsymbol{u}\|_2).$$

Remark 9 As $\boldsymbol{u}_h$ and p_h are piecewise linear and piecewise constant functions, respectively, the velocity approximation in the H^1-norm and the pressure approximation in the L^2-norm are at most first-order. From this point of view, the estimate is optimal for $\boldsymbol{u}$ and p, but not for vorticity ω for which the ideal order is three since a quadratic element is used.

4.5 Error Analysis of the $\mathrm{BDM}_1^{\mathrm{b}} - \mathrm{P}_0$ Formulation with Mass Lumping

The quadrature is exact to quadratic functions. Therefore, similar to Lemma 9, we have the first-order approximation of the discrete L^2 projection in the L^2 norm.

Lemma 14—For any quasi-uniform triangulation with size h, the discrete L^2 projection $\tilde{Q}_h: L^2 \to \sum_2^h$ satisfies

$$\|\phi - \tilde{Q}_h \phi\| \lesssim h|\phi|_1 \; for \; all \; \phi \in H^1.$$

With this first-order approximation property, we have the interpolation error estimate.

Lemma 15—Assume that $\boldsymbol{u} \in \boldsymbol{H}^2 \cap \boldsymbol{H}_0^1$. Let $\boldsymbol{u}_{\mathrm{I}}$ be the canonical interpolation of $\boldsymbol{u}$ on to the space $\mathrm{BDM}_1^{\mathrm{b}}$. Then, we have the error estimate

$$\|\mathrm{rot}\, \boldsymbol{u} - \tilde{\mathrm{rot}}_h \boldsymbol{u}_{\mathrm{I}}\| \lesssim h\|\boldsymbol{u}\|_2.$$

Theorem 7 Assume that the solution of the Stokes equations satisfies $\boldsymbol{u} \in \boldsymbol{H}^2 \cap \boldsymbol{H}_0^1$ and rot $\boldsymbol{u} \in \boldsymbol{H}^2$. Let $\boldsymbol{u}_h$ and p_h be the solution of the $\mathrm{BDM}_1^{\mathrm{b}} - \mathrm{P}_0$ approximation using formulation (2.11). Then, we have the following error estimate

$$\|\omega - \tilde{\omega}_h\| + \|\boldsymbol{u}_h - \boldsymbol{u}_{\mathrm{I}}\|_{\tilde{A}_h} + v^{-1}\|p_h - p_{\mathrm{I}}\| \lesssim h(\|\boldsymbol{u}\|_2 + \|\mathrm{rot}\, \boldsymbol{u}\|_2).$$

4.6 Improved Error Analysis of the BDM_1−P_0 and $\mathrm{BDM}_1^{\mathrm{b}} - \mathrm{P}_0$ Formulations

In this subsection, we improve the error estimates for the discrete formulation (2.8) with BDM_1−P_0 or $\mathrm{BDM}_1^{\mathrm{b}} - \mathrm{P}_0$ elements. First we present Huang and Xu's superconvergence results for the P_2 element [29]. Based on that, we obtain the improved error estimates.

Lemma 16—(Huang and Xu [29]) Assume that $\rho \in W^{3,\infty} \cap H^4 \cap H_0^1$. Suppose the triangulation $\mathcal{T}_h$ is $\mathcal{O}(h^{2\sigma})$ irregular. Let ρ_I be the quadratic Lagrange interpolation of ρ based on $\mathcal{T}_h$ Then, for any continuous and piecewise quadratic function ϕ_h,

$$|(\nabla(\rho - \rho_I), \nabla\varphi_h)| \leq h^{2+\min(1/2,\sigma)}(\|\rho\|_{4,\Omega}+|\rho|_{3,\infty,\Omega})|\varphi_h|_{1,\Omega}. \quad (4.3)$$

Lemma 17—Assume that $\boldsymbol{u} \in \boldsymbol{W}^{2,\infty} \cap \boldsymbol{H}^3 \cap \boldsymbol{H}_0^1$ div $\boldsymbol{u}$ = 0 and that the triangulation mesh is $\mathcal{O}(h^{2\sigma})$ irregular. Let $\boldsymbol{u}_I$ be the canonical interpolation of $\boldsymbol{u}$ on to BDM_1. Then, we have the error estimate

$$\|\mathrm{rot}\,\boldsymbol{u} - \mathrm{rot}_h\boldsymbol{u}_I\| \lesssim h^{1+\min(1/2,\sigma)}(\|\boldsymbol{u}\|_3+|\boldsymbol{u}|_{2,\infty}).$$

Theorem 8 Assume that the solution of the Stokes equations satisfies $\boldsymbol{u} \in \boldsymbol{W}^{2,\infty} \cap \boldsymbol{H}^3 \cap \boldsymbol{H}_0^1$ and rot $\boldsymbol{u} \in \boldsymbol{H}^3$, and that the triangulation mesh is $\mathcal{O}(h^{2\sigma})$ irregular. Let $\boldsymbol{u}_h$ and p_h be the solution of the BDM_1−P_0 approximation using formulation (2.8). Then, we have the error estimate

$$\|\omega-\omega_h\|+\|\boldsymbol{u}_h - \boldsymbol{u}_I\|_{A_h}+v^{-1}\|p_h-p_I\| \lesssim h^{1+\min(1/2,\sigma)}(\|\boldsymbol{u}\|_3+\|\boldsymbol{u}\|_{2,\infty}+|\mathrm{rot}\,\boldsymbol{u}|_3).$$

Proof One key difference between the current proof with that of Theorem 3 is that we apply the second-order approximation of Q_h to the quadratic element in the H^1 norm

$$\|\mathrm{curl}(I - Q_h)\mathrm{rot}\,\boldsymbol{u}\| \lesssim h^2|\mathrm{rot}\,\boldsymbol{u}|_3.$$

To get the corresponding error estimate for the lumped scheme $\mathrm{BDM}_1^{\mathrm{b}} - \mathrm{P}_0$ it suffices to establish the improved L^2 error estimate of the lumped L^2-projection $\tilde{Q}_h$.

Lemma 18—Assume the triangulation mesh is $\mathcal{O}(h^{2\sigma})$ irregular. The discrete L^2 projection $\tilde{Q}_h: L^2 \to \sum_2^h$ satisfies

$$\|\phi - \tilde{Q}_h\phi\| \lesssim h^{1+\min(1/2,\sigma)}|\phi|_{3/2,\infty}\, for\ all \phi \in W^{3/2,\infty}.$$

Proof We first introduce the quadratic interpolation

$$\phi_I=\sum_{i=1}^{N_V}\phi(V_i)\hat{\theta}_i+\sum_{i=1}^{N_E}\phi(E_i)\hat{\eta}_i+\sum_{\tau\in\mathscr{T}_h}\phi(C_\tau)\omega_{b,\tau}.$$

Here recall that V_i, E_i, C_τ are vertices, middle points of edges, and barycenter of triangles, respectively. And N_V, N_E are the number of total vertices and edges, respectively. The formulae of bases $\hat{\theta}_i$, $\hat{\eta}_i$, $\hat{\omega}_b$ can be found in Sect. 2.2.2. Recall that by definition

$$\tilde{Q}_h\phi=\sum_{i=1}^{N_V}\frac{(\phi,\hat{\theta}_i)}{(1,\theta_i)}\hat{\theta}_i+\sum_{i=1}^{N_E}\frac{(\phi,\hat{\eta}_i)}{(1,\eta_i)}\hat{\eta}_i+\sum_{\tau\in\mathscr{T}_h}\frac{(\phi,\omega_{b,\tau})}{(1,\omega_{b,\tau})}\omega_{b,\tau}.$$

Since the quadratic interpolation will preserve the piecewise quadratic function, we have the standard interpolation error estimate

$$\|\phi-\phi_I\|\lesssim h^{3/2}|\phi|_{3/2}.$$

So we only need to estimate the coefficients of the difference $\varphi_I - \tilde{Q_h\varphi}$.

Let $I_\tau(\varphi)=\varphi(C_\tau)-(\varphi,\omega_{b,\tau})/(1,\omega_{b,\tau})$. By direct calculation, one can easily verify $I_\tau(\lambda_i)=0$ for $i=1,2,3$, where λ_i is the basis of the linear element at vertices V_i of the triangle τ. Therefore $I_\tau(\varphi)=I_\tau(\varphi-p_1)$ for any linear polynomial p_1 and consequently by Bramble-Hilbert lemma $|I_\tau(\varphi)|\lesssim h^{3/2}|\varphi|_{3/2,\infty,\tau}$.

Let $I_E(\varphi)=\varphi(E)-(\varphi,\hat{\eta_E})/(1,\hat{\eta_E})$. Let p_1 be a linear interpolant of φ on the patch Ω_E. Then $|I_E(\varphi-p_1)|\lesssim h^{3/2}|\varphi|_{3/2,\infty,\Omega_E}$. We now estimate $|I_E(p_1)|$. It is obvious $I_E(c)=0$ for a constant. Let us use a local coordinate with original at E and check the order for $p_1=x$ or $p_1=y$. For an interior edge E, suppose $\Omega_E=\tau\cup\tau'$. Chose a quadrature rule using the triangular lattice points for polynomial of degree less than or equal to 4. We can use such a quadrature to evaluate the integral

$$(x,\hat{\eta}_E)_\tau=\sum_i x_i\hat{\eta}_E(x_i,y_i)w_i|\tau|,\ (x,\hat{\eta}_E)\tau'=\sum_i x_i'\hat{\eta}_E(x_i',y_i')w_i|\tau'|,$$

where (x_i,y_i) are quadrature points and w_i is the corresponding weight. If we write the quadrature points and $\hat{\eta_E}$ in the barycentric coordinate, it is easy to see the quantity $\hat{\eta}_E(x_i,y_i)w_i=\hat{\eta}_E(x_i',y_i')w_i$. If the patch Ω_E forms an $\mathcal{O}(h^2)$ parallelogram, then $x_i+x_i'=\mathcal{O}(h^2)$ and $|\tau|-|\tau'|=\mathcal{O}(h^3)$. Namely the patch is $\mathcal{O}(h^2)$ symmetric with respect to E_i. Therefor $I_2(p_1)\lesssim\mathcal{O}(h^2)$. For other edges, $I_E(p_1)\lesssim\mathcal{O}(h)$. But the measure of such edge patches is bounded by $\mathcal{O}(h^{2\sigma})$. Summing over all edges, we get

$$\left(\sum_E I_E^2(\phi)|\Omega_E|\right)^{1/2} \lesssim h^{1+\min(1/2,\sigma)}|\phi|_{3/2,\infty}.$$

Let $I_V(\varphi) = \varphi(V) - (\varphi, \eta\hat{V})/(1, \eta\hat{V})$. To estimate this term, we split vertices into two parts. We define $\mathcal{N}_{1,h} = \{x_i \in \mathcal{N}_h \mid$ every two neighboring triangles in Ω_i forms an $\mathcal{O}(h^2)$ approximated parallelogram$\}$, and $\mathcal{N}_{2,h} = \mathcal{N}_h \setminus \mathcal{N}_{1,h}$. For vertices x in $\mathcal{N}_{1,h}$, the patch Ω_x is $\mathcal{O}(h^2)$ symmetry. The measure $|\cup_{x\in\mathcal{N}_{2,h}}\Omega_x| \lesssim \mathcal{O}(h^{2\sigma})$. We can thus prove the estimate

$$\left(\sum_V I_V^2(\phi)|\Omega_V|\right)^2 \lesssim h^{1+\min(1/2,\sigma)}|\phi|_{3/2,\infty}$$

similarly.

The desirable estimate obtained by noticing that

$$\|\phi_I - \tilde{Q}_h\phi\|^2 \lesssim \sum_V I_V^2(\phi)|\Omega_V| + \sum_E I_E^2(\phi)|\Omega_E| + \sum_\tau I_\tau^2(\phi)|\tau|.$$

Theorem 9 Assume that the solution of the Stokes equations satisfies $\boldsymbol{u} \in \boldsymbol{W}^{2,\infty} \cap \boldsymbol{H}^3 \cap \boldsymbol{H}_0^1$ and rot $\boldsymbol{u} \in \boldsymbol{H}^3$, and that the triangulation mesh is $\mathcal{O}(h^{2\sigma})$ irregular. Let $\boldsymbol{u}_h$ and p_h be the solution of the $\mathrm{BDM}_1^{\mathrm{b}} - \mathrm{P}_0$ approximation using formulation (2.11). Then, we have the error estimate

$$\|\omega - \tilde{\omega}_h\| + \|\boldsymbol{u}_h - \boldsymbol{u}_{\mathrm{I}}\|_{\tilde{A}_h} + \upsilon^{-1}\|p_h - p_{\mathrm{I}}\| \lesssim h^{1+\min(1/2,\sigma)}(\|\boldsymbol{u}\|_3 + \|\boldsymbol{u}\|_{2,\infty} + \|\mathrm{rot}\,\boldsymbol{u}\|_3).$$

We obtain the following error estimates for the BDM_1–P_0 formulation on general unstructured grids in a way similar to that in Sect. 4.3.

Lemma 19—(Arnold et al. [2]) Let $\boldsymbol{v}_{\mathrm{II}}$ be the projection of $\boldsymbol{v}$ on to BDM_1 in Definition 6. Then, for any quasi-uniform triangulation with size h, we have the error estimate

$$(\boldsymbol{v} - \boldsymbol{v}_{\mathrm{II}}, \mathrm{curl}\,\tau) \lesssim h^{3/2}|\log h|\|\boldsymbol{v}\|_{2,\infty}\|\tau\| \; for \; all \; \tau \in \sum^h, \boldsymbol{v} \in \boldsymbol{W}^{2,\infty}.$$

Lemma 20—Assume that $\boldsymbol{u} \in \boldsymbol{W}^{2,\infty} \cap \boldsymbol{H}_0^1$ and rot $\boldsymbol{u} \in \boldsymbol{H}^2$. Let $\boldsymbol{u}_{\mathrm{II}}$ be the projection of $\boldsymbol{u}$ on to the space BDM_1 in Definition 6. Then, for any quasi-uniform triangulation with size h, we have the error estimate

$$\|\mathrm{rot}\,\boldsymbol{u} - \mathrm{rot}_h\boldsymbol{u}_{\mathrm{II}}\| \lesssim h^{3/2}(|\log h|\|\boldsymbol{u}\|_{2,\infty} + h^{1/2}|\mathscr{C}t\boldsymbol{u}|_2).$$

Theorem 10 Assume that the solution of the Stokes equations satisfies $\boldsymbol{u} \in \boldsymbol{W}^{2,\infty} \cap \boldsymbol{H}_0^1$ and rot $\boldsymbol{u} \in \boldsymbol{H}^3$. Let $\boldsymbol{u}_h$ and p_h be the solution of the BDM_1–P_0 approximation using formulation (2.8). Then, we have the following error estimate

$$\|\omega - \omega_h\| + \|\boldsymbol{u}_h - \boldsymbol{u}_{\mathrm{II}}\|_{A_h} + \nu^{-1}\|p_h - p_{\mathrm{I}}\| \lesssim h^{3/2}(|\log h|\|\boldsymbol{u}\|_{2,\infty} + h^{1/2}\|\mathrm{rot}\,\boldsymbol{u}\|_3)$$

Given the superconvergence of the pressure, we can recover the pressure from the piecewise constant to a piecewise linear function. We shall combine two methods, the least squares fitting and the harmonic averaging, both of which locally preserve linear functions. The procedure is described as follows.

We first evaluate the piecewise constant function p_h at the barycenter of each triangle. A piecewise linear pressure function p_h^r can be obtained by assigning values at vertices. This can be done by using the least square fitting to fit the piecewise constant defined on the triangles around a vertex. We will only apply the least square fitting to the boundary nodes. For the interior nodes, we construct a dual triangular mesh by connecting barycenter to the vertex, and to use it to solve a local harmonic equation. We refer to [10] for details. On the aspect of implementation, the harmonic averaging is more efficient than least square fitting for large size triangulations.

5 Numerical Experiments

In this section, we present numerical tests for both the RT_0−P_0 discretization and the $\mathrm{BDM}_1^{\mathrm{b}} - \mathrm{P}_0$ discretization. In all examples, the viscosity is chosen as one, i.e., $\nu = 1$. For both schemes, we consider three different types of grids: a criss-cross grid of the unit square, a three-directional structured grid (all triangles are formed by edges parallel to three directions only) of the unit square, and a unstructured grid of the unit disk. We refer to Figs. 1 and 2 for an illustration of these meshes. We use a uniform bisect strategy for refining the criss-cross grid. That is the triangle is bisected twice by connecting the midpoint of the longest edge to its opposite vertex. The resulting grids are still in the criss-cross type. In the so-called red refinement the triangle is divided into four congruent sub-triangles by connecting the midpoint of each edge. We use a uniform red refinement for refining the three-directional grids such that the resulting grids remains three-directional. By the $\mathcal{O}(h^{2\sigma})$ irregularity Definition 5, the three-directional structured grids correspond to $\sigma = \infty$, i.e., the $\mathcal{O}(h^2)$ approximate parallelogram property is satisfied for all pairs of adjacent triangles, and the bisection corresponds to $\sigma = 0$ since the patch of the majority of edges, which are parallel to axis, is not an $\mathcal{O}(h^2)$ approximate parallelogram. For the unstructured grids of the unit disk, we first generate a initial shape regular grid and then apply uniform red refinement. To fit the boundary, we project the boundary nodes onto the unit circle after each refinement. To improve the mesh quality, after each refinement, we apply ODT mesh optimization methods [8,11] several times. In practice these mesh optimization technique will intend to make every two adjacent triangles form an $\mathcal{O}(h^{1+\sigma})$ parallelogram and a small portion, which has a measure $\mathcal{O}(h^{2\sigma})$ of elements do not satisfy this property.

We implemented the schemes by using the MATLAB© software package *i*FEM [9].

Example 1 In the numerical tests with the unit square domain (0, 1) × (0, 1), the right-hand side $f = 0$ and the Dirichlet boundary condition for $\boldsymbol{u}$ are chosen. The analytical solutions are

$$\boldsymbol{u}(x,y)=\begin{pmatrix} 20xy^3 \\ 5x^4-5y^4 \end{pmatrix},\ p(x,y)=60x^2y-20y^3-5.$$

Example 2 In the numerical tests with the unit square domain (0, 1) × (0, 1), the Dirichlet boundary condition for $\boldsymbol{u}$ are chosen. The velocity is the same as that in Example 1 and the pressure is set zero:

$$\boldsymbol{u}(x,y)=\begin{pmatrix} 20xy^3 \\ 5x^4-5y^4 \end{pmatrix},\ p(x,y)=0,\ \boldsymbol{f}(x,y)=\begin{pmatrix} -20xy \\ -60x^2+60y^2 \end{pmatrix}.$$

Example 3 In the numerical tests with the unit disk domain centered at point (0, 0), we use the test example in [19]. The Dirichlet boundary condition for $\boldsymbol{u}$ are chosen, and the analytical solutions and the corresponding right-hand side function are

$$\boldsymbol{u}(x,y)=\begin{pmatrix} 16y-4y(x^2+y^2) \\ -16x+4x(x^2+y^2) \end{pmatrix},\ p(x,y)=0,\ \boldsymbol{f}(x,y)=\begin{pmatrix} 32y \\ -32x \end{pmatrix}.$$

We present the numerical results in Tables 1, 2, 3, 4, 5, 6, 7, 8, 9, and 10, in which N is the number of vertices of a mesh, $\boldsymbol{u}_h$, p_h, and ω_h represent the approximations; $\boldsymbol{u}_\mathrm{I}$ is the canonical interpolation of velocity $\boldsymbol{u}$; $I_h p$ is the interpolation of pressure p at the barycenters; p_h^r represents the recovered pressure; and ω_I is the nodal interpolation of vorticity ω. Based on the numerical results, we can make the following observations:

1. For criss-cross grids, the errors $\|\boldsymbol{u}_\mathrm{I}-\boldsymbol{u}_h\|_{\tilde{A}_h}$ and $\|\omega-\tilde{\mathrm{rot}}_h\boldsymbol{u}_I\|$ have no order of convergence when the RT_0–P_0 discretization is used. Both error estimates are improved to first-order, however, when the $\mathrm{BDM}_1^{\mathrm{b}}-\mathrm{P}_0$ discretization is used. This is supported by our theory since $\sigma = 0$ for criss-cross grids.
2. For three-directional girds, the errors $\|\boldsymbol{u}_\mathrm{I}-\boldsymbol{u}_h\|_{\tilde{A}_h}$ and ($\|\omega-\tilde{\mathrm{rot}}_h\boldsymbol{u}_I\|$ can achieve first-order convergence when the RT_0–P_0 discretization is used, and both increase to one and half order when the $\mathrm{BDM}_1^{\mathrm{b}}-\mathrm{P}_0$ discretization is used. This is also supported by our theory since in this case $\sigma = \infty$.
3. The error for pressure $\|p-p_h\|$ reaches half order for criss-cross grids, first order for three-directional grids when the RT_0–P_0 discretization is used, and first order for both grids when the $\mathrm{BDM}_1^{\mathrm{b}}-\mathrm{P}_0$ discretization is used. This is consistent with our theory.

4. The error for vorticity $\|\omega - \tilde{\omega_h}\|$ reaches half order for criss-cross grids and first-order for three-directional grids when the RT_0−P_0 discretization is used. It reaches one and half order for both grids when the $\mathrm{BDM}_1^{\flat} - \mathrm{P}_0$ discretization is used. The H^1 norm of the error $\|\omega_1 - \tilde{\omega_h}\|_1$ is one order less than $\|\omega_1 - \tilde{\omega_h}\|$ for all cases, which can be easily proved by the inverse inequality and the triangle inequality. In particular, for criss-cross grids, this error diverges with half order when the RT_0−P_0 discretization is used. This is consistent with our theory.

5. For Examples 1 and 2, the error for velocity and vorticity are exactly the same which demonstrates the pressure independent error estimate for velocity and vorticity.

6. For the examples on the unstructured grids of the unit disk, the error of the RT_0−P_0 discretization depends on the parameter a which measures the symmetry of edge patches. While the $\mathrm{BDM}_1^{\flat} - \mathrm{P}_0$ discretization achieves much better accuracy on the same grids and achieves the theoretical predicted order of convergence; see Tables 5 and 6.

7. We also report other norms not covered by our theory.

   - $\boldsymbol{u}_I$ and $\boldsymbol{u}_h$ are super-close in the maximum norm in all cases. A better velocity could be reconstruct based on this fact.

   - $\|\boldsymbol{u} - \boldsymbol{u}_h\|$ is first order for the RT_0−P_0 discretization, and second order for the $\mathrm{BDM}_1^{\flat} - \mathrm{P}_0$ discretization. This is reasonable, as BDM_1 contains a linear polynomial whereas RT_0 is incompletely linear.

   - $\|\boldsymbol{I}_h p - p_h\|_\infty$ and $\|\omega_I - \tilde{\omega_h}\|_\infty$ are zero order for the RT_0−P_0 discretization and first order for the $\mathrm{BDM}_1^{\flat} - \mathrm{P}_0$ discretization. Especially for the unit disk example, the computed p_h from the RT_0−P_0 discretization has no accuracy near the boundary of the disk; see the detailed explanation in [19]. The $\mathrm{BDM}_1^{\flat} - \mathrm{P}_0$ discretization, however, pushes down the error near the boundary into order $\mathcal{O}(h)$.

6 Conclusion and Future Work

We have analyzed MAC type schemes for Stokes equations using H(div) elements on unstructured triangular grids in two dimensions. When the lowest order element RT_0 is used, the rate is suboptimal on general quasi-uniform meshes. It can be improved to optimal order of convergence either by the symmetry of the mesh or by the enhancement of the velocity space to BDM_1^{b}.

In the future work, we shall extend our results in two directions. One is the non-linear Navier–Stokes equations and another is the discretization in three dimensions. For Navier–Stokes equations, we shall use the vorticity–velocity–pressure formulation $-\nu\Delta\boldsymbol{u} + \omega \times \boldsymbol{u} + \Delta(p + |\boldsymbol{u}|^2/2) = \boldsymbol{f}$ and replace the vorticity $\omega = \tilde{\mathrm{rot}}_h \boldsymbol{u}$. We shall follow [39] to establish some energy estimate first and then derive corresponding error estimate.

Generalization to three dimensions is much harder since now the space for the vorticity is the edge element space. Mass lumping for the edge element space is not obvious. And supreconvergence results for edge element spaces are rare [32,33]. We may need to work on different discretizations using the vorticity–velocity–pressure formulation. For example, results on three dimensional co-volume methods for Stokes and Maxwell's equations can be found in [38,40] and least-square formulation for the three dimensional Stokes equations based on the vorticity-velocity-pressure formulation can be found in [17].

Acknowledgments

The authors Long Chen and Lin Zhong was supported by NSF Grant DMS-1115961, and in part by Department of Energy prime award # DE-SC0006903, NSF grant DMS-1161621 and NIH grant P50GM76516. The work of the author Ming Wang was supported by 2010–2012 China Scholarship Council (CSC).

References

1. Arnold D, Falk R, Winther R. Finite element exterior calculus: from hodge theory to numerical stability. Am Math Soc. 2010; 47:281–354.
2. Arnold DN, Falk RS, Gopalakrishnan J. Mixed finite element approximation of the vector Laplacian with Dirichlet boundary conditions. Math Models Methods Appl Sci. 2012; 22(09)
3. Arnold DN, Falk RS, Guzmán J, Tsogtgerel G. On the consistency of the combinatorial codifferential. T Am Math Soc. 2014; 366(10):5487–5502.
4. Bank RE, Xu J. Asymptotically exact a posteriori error estimators, part I: grids with superconvergence. SIAM J Numer Anal. 2003; 41(6):2294–2312.
5. Baranger J, Maitre JF, Oudin F. Connection between finite volume and mixed finite element methods. ESAIM: Math Model Numer Anal. 1996; 30(4):445–465.
6. Brandt, A.; Dinar, N. Multi-grid solutions to elliptic flow problems In: Institute for Computer Applications in Science and Engineering. NASA Langley Research Center; 1979.
7. Carrero J, Cockburn B, Schötzau D. Hybridized globally divergence-free LDG methods. part I: the stokes problem. Math Comput. 2006; 75(254):533–564.
8. Chen, L. 13th International Meshing Roundtable. Williamsburg, VA: Sandia National Laboratories; 2004. Mesh smoothing schemes based on optimal Delaunay triangulations; p. 109-120.2004
9. Chen, L. Technical Report. University of California at Irvine; 2009. *i*FEM: an integrated finite element methods package in MATLAB.
10. Chen L, Cai Y. A unified construction of barycentric coordinates on polygons. Preparation. 2013
11. Chen L, Holst MJ. Efficient mesh optimization schemes based on optimal Delaunay Triangulations. Comput Methods Appl Mech Eng. 2011; 200:967–984.
12. Chen, L.; Wang, M.; Zhong, L. Technical Report. University of California at Irvine; 2013. Second order accuracy of a MAC scheme for the steady state Stokes equations.
13. Choudhury S, Nicolaides R. Discretization of incompressible vorticity–velocity equations on triangular meshes. Int J Numer Methods Fluids. 1990; 11(6):823–833.
14. Cockburn B, Gopalakrishnan J. The derivation of hybridizable discontinuous Galerkin methods for Stokes flow. SIAM J Numer Anal. 2009; 47(2):1092–1125.
15. Cockburn B, Kanschat G, Schötzau D, Schwab C. Local discontinuous Galerkin methods for the Stokes system. SIAM J Numer Anal. 2002; 40(1):319–343.
16. Cohen G, Joly P, Roberts J, Tordjman N. Higher order triangular finite elements with mass lumping for the wave equation. SIAM J Numer Anal. 2001; 38(6):2047–2078.
17. Duan HY, Liang GP. On the velocity-pressure-vorticity least-squares mixed finite element method for the 3D Stokes equations. SIAM J Numer Anal. 2003; 41(6):2114–2130.
18. Dubois F. Vorticity–velocity-pressure formulation for the Stokes problem. Math Methods Appl Sci. 2002; 25(13):1091–1119.

19. Dubois F, Salaun M, Salmon S. First vorticity–velocity-pressure numerical scheme for the Stokes problem. Comput Methods Appl Mech Eng. 2003; 192(44–46):4877–4907.
20. Dubois F, Salaün M, Salmon S. Vorticity–velocity-pressure and stream function-vorticity formulations for the Stokes problem. J de Math Pures et Appliquées. 2003; 82(11):1395–1451.
21. Eymard R, Fuhrmann J, Linke A. On MAC schemes on triangular delaunay meshes, their convergence and application to coupled flow problems. Numer Methods Partial Differ Equ. 2011; 30(4):1397–1424.
22. Falk R, Neilan M. Stokes complexes and the construction of stable finite elements with pointwise mass conservation. SIAM J Numer Anal. 2013; 51(2):1308–1326.
23. Girault V, Lopez H. Finite-element error estimates for the MAC scheme. IMA J Numer Anal. 1996; 16(3):347–379.
24. Girault, V.; Raviart, P. Finite Element Methods for Navier–Stokes Equations: Theory and Algorithms, volume 5 of Springer Series in Computational Mathematics. Vol. 87. Springer; Berlin: 1986. p. 52227
25. Guzmán J, Neilan M. Conforming and divergence free Stokes elements on general triangular meshes. Math Comput. 2011; 83:15–36.
26. Han H, Wu X. A new mixed finite element formulation and the MAC method for the Stokes equations. IAM J Numer Anal. 1998; 35:560–571.
27. Harlow FH, Welch JE. Numerical calculation of time-dependent viscous incompressible flow of fluid with free surface. Phys Fluids. 1965; 8:2182.
28. Hiptmair R. Finite elements in computational electromagnetism. Acta Numer. 2002; 11:237–339.
29. Huang Y, Xu J. Superconvergence of quadratic finite elements on mildly structured grids. Math Comput. 2008; 77(263):1253–1268.
30. Kanschat G. Divergence-free discontinuous Galerkin schemes for the Stokes equations and the MAC scheme. Int J Numer Methods Fluids. 2008; 56(7):941–950.
31. Lakhany AM, Marek I, Whiteman JR. Superconvergence results on mildly structured triangulations. Comput Methods Appl Mech Eng. 2000; 189:1–75.
32. Lin Q, Li J. Superconvergence analysis for Maxwell's equations in dispersive media. Math Comput. 2008; 77(262):757.
33. Lin Q, Yan N. Global superconvergence for Maxwell's equations. Math Comput. 2000; 69(229): 159–176.
34. Minev P. Remarks on the links between low-order DG methods and some finite-difference schemes for the Stokes problem. Int J Numer Methods Fluids. 2008; 58(3):307–317.
35. Nédélec J. A new family of mixed finite elements in R^3. Numer Math. 1986; 50(1):57–81.
36. Nicolaides R. Flow discretization by complementary volume techniques. 9th AIAA Computational Fluid Dynamics Conference. 1989; 1:464–470.
37. Nicolaides R. Analysis and convergence of the MAC scheme I. The linear problem. SIAM J Numer Anal. 1992; 29(6):1579–1591.
38. Nicolaides RA, Wang DQ. Convergence analysis of a covolume scheme for Maxwell's equations in three dimensions. Math Comput. 1998; 67(223):947–964.
39. Nicolaides R, Wu X. Analysis and convergence of the MAC scheme. II. Navier–Stokes equations. Math Comput. 1996; 65(213):29–44.
40. Nicolaides RA, Wu X. Covolume solutions of three dimensional div-curl equations. SIAM J Numer Anal. 1997; 34(6):1406–1419.
41. Oosterlee C, Lorenz F. Multigrid methods for the Stokes system. Comput Sci Eng. 2006; 8(6):34–43.
42. Perot JB. Conservation properties of unstructured staggered mesh schemes. J Comput Phys. 2000; 159(1):58–89.
43. Perot JB. Discrete conservation properties of unstructured mesh schemes. Annu Rev Fluid Mech. 2011; 43:299–318.
44. Taylor C, Hood P. A numerical solution of the Navier–Stokes equations using the finite element technique. Comput Fluids. 1973; 1:73–100.

45. Wang J, Wang Y, Ye X. A new finite volume method for the Stokes problems. Int J Numer Anal Model. 2009; 7:281–302.
46. Wang J, Ye X. New finite element methods in computational fluid dynamics by H(div) elements. SIAM J Numer Anal. 2007; 45(3):1269–1286.
47. Wang M, Chen L. Multigrid methods for the Stokes equations using distributive Gauss–Seidel relaxations based on the least squares commutator. J Sci Comput. 2013; 56(2):409–431.
48. Wittum G. Multi-grid methods for Stokes and Navier–Stokes equations. Numer Math. 1989; 54(5): 543–563.
49. Xu J, Zhang ZM. Analysis of recovery type a posteriori error estimators for mildly structured grids. Math Comput. 2004; 73(247):1139–1152.

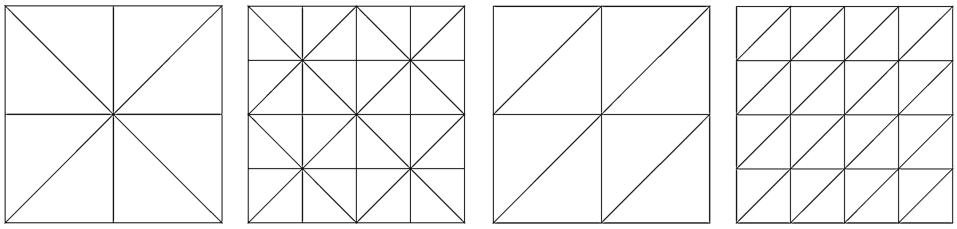

Fig. 1. Criss-cross grids and three-directional structured grids of a square domain

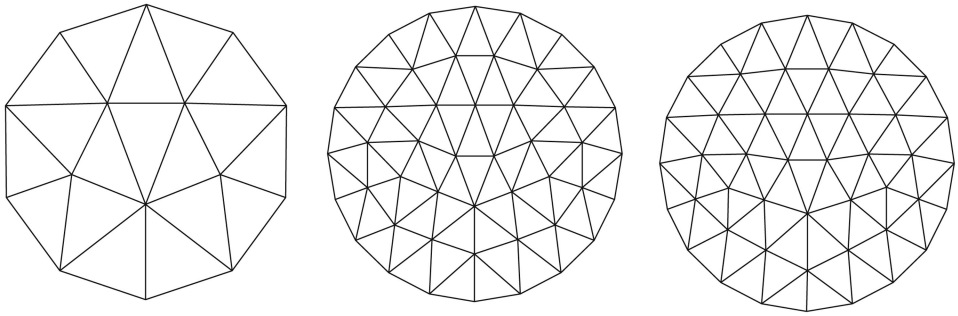

Fig. 2. Unstructured grids of a disk domain

Table 1

Example 1: errors for the RT_0–P_0 element discretization on criss−cross grids

N	$\|\|u_I - u_h\|\|_{\tilde{A}_h}$	$\|\|u_I - u_h\|\|$	$\|\|u - u_h\|\|$	$\|\|u_I - u_h\|\|_\infty$
289	3.899*e*+00	8.615*e*−02	4.065*e*−01	1.742*e*−02
1,089	4.021*e*+00	4.337*e*−02	2.028*e*−01	4.572*e*−03
4,225	4.082*e*+00	2.176*e*−02	1.013*e*−01	1.169*e*−03
16,641	4.111*e*+00	1.090*e*−02	5.063*e*−02	2.954*e*−04
Order	−0.017	1.013	1.018	2.010
N	$\|\|I_h p - p_h\|\|$	$\|\|p - p_h\|\|$	$\|\|p - p_h^r\|\|$	$\|\|I_h p - p_h\|\|_\infty$
289	9.873*e*−01	1.208*e*+00	3.910*e*−01	8.660*e*+00
1,089	6.525*e*−01	7.396*e*−01	1.208*e*−01	7.215*e*+00
4,225	4.499*e*−01	4.824*e*−01	4.573*e*−02	6.801*e*+00
16,641	3.144*e*−01	3.262*e*−01	2.211*e*−02	6.581*e*+00
Order	0.536	0.600	1.246	0.067
N	$\|\|\omega_I - \tilde{\omega_h}\|\|_1$	$\|\|\omega - \tilde{\omega_h}\|\|$	$\|\|\omega - \widetilde{\mathrm{rot}}_h u_I\|\|$	$\|\|\omega_I - \tilde{\omega_h}\|\|_\infty$
289	6.406*e*+01	1.134*e*+00	2.243*e*+00	3.048*e*+01
1,089	8.195*e*+01	6.860*e*−01	2.113*e*+00	3.024*e*+01
4,225	1.091*e*+02	4.421*e*−01	2.081*e*+00	3.012*e*+01
16,641	1.491*e*+02	2.968*e*−01	2.073*e*+00	3.006*e*+01
Order	−0.439	0.614	0.014	0.004

Table 2

Example 2: errors for the RT_0−P_0 element discretization on criss-cross grids

N	$\|\|u_I - u_h\|\|_{\tilde{A}_h}$	$\|\|u_I - u_h\|\|$	$\|\|u - u_h\|\|$	$\|\|u_I - u_h\|\|_\infty$
289	3.899*e*+00	8.615*e*−02	4.065*e*−01	1.742*e*−02
1,089	4.021*e*+00	4.337*e*−02	2.028*e*−01	4.572*e*−03
4,225	4.082*e*+00	2.176*e*−02	1.013*e*−01	1.169*e*−03
16,641	4.111*e*+00	1.090*e*−02	5.063*e*−02	2.954*e*−04
Order	−0.017	1.013	1.018	2.010
N	$\|\|I_h p - p_h\|\|$	$\|\|p - p_h\|\|$	$\|\|p - p_h^r\|\|$	$\|\|I_h p - p_h\|\|_\infty$
289	9.865*e*−01	9.865*e*−01	2.858*e*−01	8.672*e*+00
1,089	6.523*e*−01	6.523*e*−01	9.751*e*−02	7.212*e*+00
4,225	4.498*e*−01	4.498*e*−01	4.191*e*−02	6.800*e*+00
16,641	3.144*e*−01	3.143*e*−01	2.167*e*−02	6.580*e*+00
Order	0.535	0.535	1.103	0.067
N	$\|\|\omega_I - \tilde{\omega_h}\|\|_1$	$\|\|\omega - \tilde{\omega_h}\|\|$	$\|\|\omega - \widetilde{\mathrm{rot}}_h u_I\|\|$	$\|\|\omega_I - \tilde{\omega_h}\|\|_\infty$
289	6.406*e*+01	1.134*e*+00	2.243*e*+00	3.048*e*+01
1,089	8.195*e*+01	6.860*e*−01	2.113*e*+00	3.024*e*+01
4,225	1.091*e*+02	4.421*e*−01	2.081*e*+00	3.012*e*+01
16,641	1.491*e*+02	2.968*e*−01	2.073*e*+00	3.006*e*+01
Order	−0.439	0.614	0.014	0.004

Table 3

Example 1: errors for the RT_0−P_0 element discretization on three-directional grids

N	$\|\|u_I - u_h\|\|_{\tilde{A}_h}$	$\|\|u_I - u_h\|\|$	$\|\|u - u_h\|\|$	$\|\|u_I - u_h\|\|_\infty$
289	2.491e−01	1.273e−02	4.683e−01	2.157e−03
1,089	1.041e−01	3.397e−03	2.344e−01	3.601e−04
4,225	4.045e−02	8.683e−04	1.172e−01	5.364e−05
16,641	1.510e−02	2.187e−04	5.862e−02	7.501e−06
Order	1.416	2.012	1.017	2.840
N	$\|\|I_h p - p_h\|\|$	$\|\|p - p_h\|\|$	$\|\|p - p_h^r\|\|$	$\|\|I_h p - p_h\|\|_\infty$
289	5.018e−01	8.590e−01	4.951e−01	9.077e+00
1,089	1.993e−01	4.016e−01	1.745e−01	7.264e+00
4,225	8.640e−02	1.945e−01	6.786e−02	6.199e+00
16,641	4.048e−02	9.610e−02	2.980e−02	5.619e+00
Order	1.169	1.049	1.296	0.188
N	$\|\|\omega_I - \tilde{\omega_h}\|\|_1$	$\|\|\omega - \tilde{\omega_h}\|\|$	$\|\|\omega - \widetilde{\mathrm{rot}}_h u_I\|\|$	$\|\|\omega_I - \tilde{\omega_h}\|\|_\infty$
289	5.050e+01	1.083e+00	1.093e+00	3.909e+01
1,089	5.068e+01	5.358e−01	5.407e−01	3.954e+01
4,225	5.082e+01	2.670e−01	2.687e−01	3.977e+01
16,641	5.090e+01	1.334e−01	1.339e−01	3.988e+01
Order	−0.006	1.020	1.024	−0.006

Table 4

Example 2: errors for the RT_0−P_0 element discretization on three-directional grids

N	$\|\|u_I - u_h\|\|_{\tilde{A}_h}$	$\|\|u_I - u_h\|\|$	$\|\|u - u_h\|\|$	$\|\|u_I - u_h\|\|_\infty$
289	2.491e−01	1.273e−02	4.683e−01	2.157e−03
1,089	1.041e−01	3.397e−03	2.344e−01	3.601e−04
4,225	4.045e−02	8.683e−04	1.172e−01	5.364e−05
16,641	1.510e−02	2.187e−04	5.862e−02	7.501e−06
Order	1.416	2.012	1.017	2.840
N	$\|\|I_h p - p_h\|\|$	$\|\|p - p_h\|\|$	$\|\|p - p_h^r\|\|$	$\|\|I_h p - p_h\|\|_\infty$
289	5.025e−01	5.025e−01	4.451e−01	9.089e+00
1,089	1.995e−01	1.995e−01	1.650e−01	7.267e+00
4,225	8.642e−02	8.642e−02	6.629e−02	6.200e+00
16,641	4.048e−02	4.048e−02	2.957e−02	5.619e+00
Order	1.169	1.169	1.261	0.188
N	$\|\|\omega_I - \tilde{\omega_h}\|\|_1$	$\|\|\omega - \tilde{\omega_h}\|\|$	$\|\|\omega - \widetilde{\mathrm{rot}}_h u_I\|\|$	$\|\|\omega_I - \tilde{\omega_h}\|\|_\infty$
289	5.050e+01	1.083e+00	1.093e+00	3.909e+01
1,089	5.068e+01	5.358e−01	5.407e−01	3.954e+01
4,225	5.082e+01	2.670e−01	2.687e−01	3.977e+01
16,641	5.090e+01	1.334e−01	1.339e−01	3.988e+01
Order	−0.006	1.020	1.024	−0.006

Table 5

Example 1: errors for the $\mathrm{BDM}_1^{\mathrm{b}} - \mathrm{P}_0$ element discretization on criss-cross grids

N	$\|\boldsymbol{u}_{\mathrm{I}} - \boldsymbol{u}_h\|_{\tilde{A}_h}$	$\|\boldsymbol{u}_{\mathrm{I}} - \boldsymbol{u}_h\|$	$\|\boldsymbol{u} - \boldsymbol{u}_h\|$	$\|\boldsymbol{u}_{\mathrm{I}} - \boldsymbol{u}_h\|_\infty$
289	2.836*e*−01	3.544*e*−03	1.088*e*−02	1.228*e*−03
1,089	1.393*e*−01	8.724*e*−04	2.710*e*−03	1.630*e*−04
4,225	6.903*e*−02	2.161*e*−04	6.763*e*−04	2.099*e*−05
16,641	3.436*e*−02	5.374*e*−05	1.689*e*−04	2.663*e*−06
Order	1.026	2.044	2.035	3.018
N	$\|I_h p - p_h\|$	$\|p - p_h\|$	$\|\|p - p_h^r\|\|$	$\|I_h p - p_h\|_\infty$
289	3.925*e*−02	6.977*e*−01	1.760*e*−01	2.282*e*−01
1,089	1.381*e*−02	3.488*e*−01	5.347*e*−02	1.125*e*−01
4,225	4.881*e*−03	1.744*e*−01	1.704*e*−02	5.582*e*−02
16,641	1.726*e*−03	8.717*e*−02	5.659*e*−03	2.779*e*−02
Order	1.525	1.017	1.647	1.026
N	$\|\omega_{\mathrm{I}} - \tilde{\omega_h}\|_1$	$\|\omega - \tilde{\omega_h}\|$	$\|\|\omega - \widetilde{\mathrm{rot}}_h u_{\mathrm{I}}\|\|$	$\|\omega_{\mathrm{I}} - \tilde{\omega_h}\|_\infty$
289	1.150*e*+01	1.235*e*−01	5.504*e*−01	2.750*e*+00
1,089	8.064*e*+00	4.352*e*−02	2.703*e*−01	1.397*e*+00
4,225	5.675*e*+00	1.536*e*−02	1.339*e*−01	7.044*e*−01
16,641	4.003*e*+00	5.423*e*−03	6.662*e*−02	3.536*e*−01
Order	0.513	1.527	1.027	1.008

Table 6

Example 2: Errors for the $\mathrm{BDM}_1^{\mathrm{b}} - \mathrm{P}_0$ element discretization on criss-cross grids

N	$\|\boldsymbol{u}_{\mathrm{I}} - \boldsymbol{u}_h\|_{\tilde{A}_h}$	$\|\boldsymbol{u}_{\mathrm{I}} - \boldsymbol{u}_h\|$	$\|\boldsymbol{u} - \boldsymbol{u}_h\|$	$\|\boldsymbol{u}_{\mathrm{I}} - \boldsymbol{u}_h\|_\infty$
289	2.836*e*−01	3.544*e*−03	1.088*e*−02	1.228*e*−03
1,089	1.393*e*−01	8.724*e*−04	2.710*e*−03	1.630*e*−04
4,225	6.903*e*−02	2.161*e*−04	6.763*e*−04	2.099*e*−05
16,641	3.436*e*−02	5.374*e*−05	1.689*e*−04	2.663*e*−06
Order	1.026	2.044	2.035	3.018
N	$\|I_h p - p_h\|$	$\|p - p_h\|$	$\|\|p - p_h^r\|\|$	$\|I_h p - p_h\|_\infty$
289	3.870*e*−02	3.870*e*−01	4.212*e*−02	2.155*e*−01
1,089	1.372*e*−02	1.372*e*−02	1.577*e*−02	1.093*e*−01
4,225	4.865*e*−03	4.865*e*−03	5.735*e*−03	5.501*e*−02
16,641	1.724*e*−03	1.724*e*−03	2.056*e*−03	2.758*e*−02
Order	1.521	1.521	1.495	1.010
N	$\|\omega_{\mathrm{I}} - \tilde{\omega_h}\|_1$	$\|\omega - \tilde{\omega_h}\|$	$\|\|\omega - \widetilde{\mathrm{rot}}_h u_{\mathrm{I}}\|\|$	$\|\omega_{\mathrm{I}} - \tilde{\omega_h}\|_\infty$
289	1.150*e*+01	1.235*e*−01	5.504*e*−01	2.750*e*+00
1,089	8.064*e*+00	4.352*e*−02	2.703*e*−01	1.397*e*+00
4,225	5.675*e*+00	1.536*e*−02	1.339*e*−01	7.044*e*−01
16,641	4.003*e*+00	5.423*e*−03	6.662*e*−02	3.536*e*−01
Order	0.513	1.527	1.027	1.008

Table 7

Example 1: errors for the $\mathrm{BDM}_1^{\mathrm{b}} - \mathrm{P}_0$ element discretization on three-directional grids

N	$\|\boldsymbol{u}_{\mathrm{I}} - \boldsymbol{u}_h\|_{\tilde{A}_h}$	$\|\boldsymbol{u}_{\mathrm{I}} - \boldsymbol{u}_h\|$	$\|\boldsymbol{u} - \boldsymbol{u}_h\|$	$\|\boldsymbol{u}_{\mathrm{I}} - \boldsymbol{u}_h\|_\infty$
289	1.414*e*−01	1.529*e*−03	1.326*e*−02	5.706*e*−04
1,089	4.719*e*−02	2.635*e*−04	3.308*e*−03	7.215*e*−05
4,225	1.606*e*−02	4.561*e*−05	8.261*e*−04	9.062*e*−06
16,641	5.555*e*−03	8.018*e*−06	2.064*e*−04	1.135*e*−06
Order	1.569	2.561	2.035	3.045
N	$\|I_h p - p_h\|$	$\|p - p_h\|$	$\|\|p - p_h^r\|\|$	$\|I_h p - p_h\|_\infty$
289	7.021*e*−02	7.001*e*−01	1.372*e*−01	9.643*e*−01
1,089	2.224*e*−02	3.492*e*−01	4.100*e*−02	4.928*e*−01
4,225	7.308*e*−03	1.744*e*−01	1.290*e*−02	2.488*e*−01
16,641	2.475*e*−03	8.719*e*−02	4.243*e*−03	1.250*e*−01
Order	1.610	1.018	1.663	1.006
N	$\|\omega_{\mathrm{I}} - \tilde{\omega_h}\|_1$	$\|\omega - \tilde{\omega_h}\|$	$\|\|\omega - \widetilde{\mathrm{rot}}_h u_{\mathrm{I}}\|\|$	$\|\omega_{\mathrm{I}} - \tilde{\omega_h}\|_\infty$
289	2.300*e*+01	1.960*e*−01	3.259*e*−01	2.947*e*+00
1,089	1.662*e*+01	7.086*e*−02	1.174*e*−01	1.512*e*+00
4,225	1.187*e*+01	2.532*e*−02	4.192*e*−02	7.659*e*−01
16,641	8.440*e*+00	9.000*e*−03	1.489*e*−02	3.854*e*−01
Order	0.497	1.513	1.514	1.002

Table 8

Example 2: errors for the $\mathrm{BDM}_1^{\mathrm{b}} - \mathrm{P}_0$ element discretization on three-directional grids

N	$\|\boldsymbol{u}_{\mathrm{I}} - \boldsymbol{u}_h\|_{\tilde{A}_h}$	$\|\boldsymbol{u}_{\mathrm{I}} - \boldsymbol{u}_h\|$	$\|\boldsymbol{u} - \boldsymbol{u}_h\|$	$\|\boldsymbol{u}_{\mathrm{I}} - \boldsymbol{u}_h\|_\infty$
289	1.414*e*−01	1.529*e*−03	1.326*e*−02	5.706*e*−04
1,089	4.719*e*−02	2.635*e*−04	3.308*e*−03	7.215*e*−05
4,225	1.606*e*−02	4.561*e*−05	8.261*e*−04	9.062*e*−06
16,641	5.555*e*−03	8.018*e*−06	2.064*e*−04	1.135*e*−06
Order	1.569	2.561	2.035	3.045
N	$\|I_h p - p_h\|$	$\|p - p_h\|$	$\|p - p_h^r\|$	$\|I_h p - p_h\|_\infty$
289	6.993*e*−02	6.993*e*−02	1.169*e*−01	9.581*e*−01
1,089	2.220*e*−02	2.220*e*−02	3.705*e*−02	4.912*e*−01
4,225	7.301*e*−03	7.301*e*−03	1.215*e*−02	2.484*e*−01
16,641	2.474*e*−03	2.474*e*−03	4.105*e*−03	1.249*e*−01
Order	1.609	1.609	1.614	1.005
N	$\|\omega_{\mathrm{I}} - \tilde{\omega_h}\|_1$	$\|\omega - \tilde{\omega_h}\|$	$\|\omega - \widetilde{\mathrm{rot}}_h u_{\mathrm{I}}\|$	$\|\omega_{\mathrm{I}} - \tilde{\omega_h}\|_\infty$
289	2.300*e*+01	1.960*e*−01	3.259*e*−01	2.947*e*+00
1,089	1.662*e*+01	7.086*e*−02	1.174*e*−01	1.512*e*+00
4,225	1.187*e*+01	2.532*e*−02	4.192*e*−02	7.659*e*−01
16,641	8.440*e*+00	9.000*e*−03	1.489*e*−02	3.854*e*−01
Order	0.497	1.513	1.514	1.002

Table 9

Example 3: Errors for the RT_0–P_0 element discretization on unstructured grids of the unit disk

N	$\|\|u_I - u_h\|\|_{\tilde{a}_h}$	$\|\|u_I - u_h\|\|$	$\|\|u - u_h\|\|$	$\|\|u_I - u_h\|\|_\infty$
194	1.753*e*+00	1.622*e*−01	9.720*e*−01	3.223*e*−02
727	7.453*e*−01	4.245*e*−02	4.844*e*−01	5.701*e*−03
2,813	3.397*e*−01	1.096*e*−02	2.420*e*−01	1.198*e*−03
11,065	1.630*e*−01	2.815*e*−03	1.210*e*−01	2.756*e*−04
Order	1.116	1.993	1.019	2.225
N	$\|\|I_h p - p_h\|\|$	$\|\|p - p_h\|\|$	$\|\|p - p_h^r\|\|$	$\|\|I_h p - p_h\|\|_\infty$
194	3.871*e*−01	3.871*e*−01	2.434*e*−01	1.153*e*+00
727	2.892*e*−01	2.892*e*−01	1.320*e*−01	1.695*e*+00
2,813	1.699*e*−01	1.699*e*−01	9.116*e*−02	1.790*e*+00
11,065	8.831*e*−02	8.831*e*−02	5.140*e*−02	1.802*e*+00
Order	0.871	0.871	0.693	−0.045
N	$\|\|\omega_I - \tilde{\omega_h}\|\|_1$	$\|\|\omega - \tilde{\omega_h}\|\|$	$\|\|\omega - \widetilde{\mathrm{rot}}_h u_1\|\|$	$\|\|\omega_I - \tilde{\omega_h}\|\|_\infty$
194	7.664*e*+00	3.639*e*−01	1.350*e*+00	2.762*e*+00
727	1.432*e*+01	2.630*e*−01	6.126*e*−01	3.941*e*+00
2,813	1.497*e*+01	1.589*e*−01	2.910*e*−01	4.311*e*+00
11,065	1.503*e*+01	8.289*e*−02	1.416*e*−01	4.401*e*+00
Order	−0.035	0.848	1.076	−0.081

Table 10

Example 3: errors for the $\mathrm{BDM}_1^{\mathrm{b}} - \mathrm{P}_0$ element discretization on unstructured grids of the unit disk

N	$\|\|u_I - u_h\|\|_{\tilde{A}_h}$	$\|\|u_I - u_h\|\|$	$\|\|u - u_h\|\|$	$\|\|u_I - u_h\|\|_\infty$
194	2.018*e*−01	4.302*e*−03	2.152*e*−02	1.616*e*−03
727	6.932*e*−02	7.531*e*−04	5.358*e*−03	2.419*e*−04
2,813	2.498*e*−02	1.372*e*−04	1.337*e*−03	3.354*e*−05
11,065	9.041*e*−03	2.483*e*−05	3.339*e*−04	4.237*e*−06
Order	1.496	2.506	2.038	2.971
N	$\|\|I_h p - p_h\|\|$	$\|\|p - p_h\|\|$	$\|\|p - p_h^r\|\|$	$\|\|I_h p - p_h\|\|_\infty$
194	3.010*e*−02	3.010*e*−02	4.375*e*−02	1.028*e*−01
727	1.205*e*−02	1.205*e*−02	2.014*e*−02	6.260*e*−02
2,813	4.666*e*−03	4.666*e*−03	7.872*e*−03	3.234*e*−02
11,065	1.731*e*−03	1.731*e*−03	2.914*e*−03	1.639*e*−02
Order	1.426	1.426	1.420	0.984
N	$\|\|\omega_I - \omega_h\|\|_1$	$\|\|\omega - \omega_h\|\|$	$\|\|\omega - \widetilde{\mathrm{rot}}_h u_I\|\|$	$\|\|\omega_I - \omega_h\|\|_\infty$
194	1.105*e*+01	2.114*e*−01	2.701*e*−01	9.710*e*−01
727	8.025*e*+00	7.654*e*−02	1.008*e*−01	5.067*e*−01
2,813	5.765*e*+00	2.731*e*−02	3.655*e*−02	2.572*e*−01
11,065	4.110*e*+00	9.702*e*−03	1.308*e*−02	1.294*e*−01
Order	0.491	1.517	1.500	1.002